Middle Atmosphere Dynamics with Gravity Wave Interactions in the Numerical Spectral Model: Tides and Planetary Waves

H. G. Mayr[1], J. G. Mengel[2†], K. L. Chan[3], and F. T. Huang[4]
[1] Goddard Space Flight Center, Greenbelt, MD, USA
[2] Science Systems and Applications Inc., Lanham, MD, USA
[3] University of Science and Technology, Hong Kong, China
[4] University of Maryland, Baltimore, MD, USA
† Deceased

Corresponding Author:
Hans G. Mayr
hans.g.mayr@nasa.gov
hmayr2@verizon.net
Goddard Space Flight Center
Laboratory for Atmospheres, Code 613.3
8800 Greenbelt Road
Greenbelt, MD, 20771
USA

Manuscript
For
Journal of Atmospheric and Solar Terrestrial Physics
September 8, 2010

Abstract: As Lindzen (1981) had shown, small-scale gravity waves (GW) produce the observed reversals of the zonal-mean circulation and temperature variations in the upper mesosphere. The waves also play a major role in modulating and amplifying the diurnal tides (DT) (e.g., Waltersheid, 1981; Fritts and Vincent, 1987; Fritts, 1995a). We summarize here the modeling studies with the mechanistic numerical spectral model (NSM) with Doppler spread parameterization for GW (Hines, 1997a, b), which describes in the middle atmosphere: (a) migrating and non-migrating DT, (b) planetary waves (PW), and (c) global-scale inertio gravity waves. Numerical experiments are discussed that illuminate the influence of GW filtering and nonlinear interactions between DT, PW, and zonal mean variations.

Keywords: Theoretical modeling, Middle atmosphere dynamics, Gravity wave interactions, Migrating and non-migrating tides, Planetary waves, Global-scale inertio gravity waves.

1. Introduction

The fundamental properties of diurnal tides (DT) and planetary waves (PW) are well understood (Chapman and Lindzen, 1970; Holton, 1979; Kato, 1980; Volland, 1988). Measurements from the ground and with spacecraft have shown that the DT in the mesosphere and lower thermosphere exhibit large seasonal and inter-annual variations, and that they are modulated by PW (e.g., Avery et al., 1989; Manson et al., 1989; Vincent et al., 1989; Gille et al., 1991; Hays et al., 1994; Burrage et al., 1995a, b; McLandress et al., 1996; Wu et al., 1998; Leblanc et al., 1999a, b; Huang and Reber, 2003, 2004; Wu and Jiang, 2005; Zhang et al., 2006; Muktarov et al., 2009; Huang et al., 2006, 2010).

In the mesosphere, the DT, PW, and small-scale gravity waves (GW) attain large amplitudes, and their interactions have been the subject of theoretical studies (e.g., Walterscheid, 1981; Fritts, 1984, 1995a, b; Fritts and Vincent, 1987; Vial and Forbes, 1989; Forbes et al., 1991; Forbes, 1995). Numerical models have been employed to study the DT under the influence of the zonal-mean circulation, eddy viscosity, and GW interactions (e.g., Lindzen and Hong, 1974; Forbes and Hagan, 1988; Forbes and Vial, 1989; Akmaev et al., 1996; Miyahara and Forbes, 1991; Hagan, 1996; Hagan et al., 1993, 1995, 1999a; Yudin et al., 1997; McLandress, 1997a, 2002a, b; Miyahara et al., 1993, 1999; Geller et al., 1997; Mayr et al., 1998; Akmaev, 2001a, b).

Mayr et al. (2010), referred to as MMCH, summarize the zonal-mean variations in the middle atmosphere, which are generated in the numerical spectral model (NSM) with parameterized GW. In this companion paper, we discuss the tides, planetary waves, and global-scale inertio gravity waves.

Chan et al. (1994, 1995) introduced the NSM, which is fully nonlinear and is integrated from the surface into the thermosphere. Formulated in terms of vector spherical harmonics, the model allows us to study the individual and interacting dynamical components with zonal wave numbers m = 0 to 4, as illustrated in Fig. 1 of MMCH. The zonal-mean (m = 0) heating rates for the middle atmosphere are taken from Strobel (1978), and the excitation rates for the migrating DT in the troposphere and stratosphere are taken from Forbes and Garrett (1978). Solar EUV heating is applied in the thermosphere. The planetary waves (PW) are generated internally by instabilities. Newtonian cooling describes radiative loss (Wehrbein and Leovy, 1982; Zhu, 1989). Starting with Mengel et al. (1995), the NSM has been run with the Doppler spread parameterization (DSP) for GW developed by Hines (1997a, b). In the DSP formulation, GW momentum is strictly conserved, which is important for wave filtering and the associated nonlinear interactions. The DSP comes with uncertainties that affect the height dependent GW momentum source and eddy viscosity, and the input parameters were changed over the years as documented in the literature. In all DSP applications, for simplicity, the GW source at the initial height was chosen to be isotropic, time independent, and hemispherically symmetric.

By way of introduction, we present in Fig. 1 numerical results from 2D (a) and 3D (b) versions of the NSM. Applying the same GW source at the initial height, the zonal-mean (m = 0) winds are

presented, which describe the quasi-biennial oscillation (QBO) and semi-annual oscillation (SAO) near the equator. From the 2D model (Fig. 1a), the wind velocities are much larger than those in 3D (Fig. 1b). The GW in 2D are solely available to generate and amplify the QBO and SAO. In the 3D model, the GW apparently amplify the tides and planetary waves at the expense of the equatorial oscillations. This illustrates how GW interactions can influence, and couple, the dynamical components of the atmosphere.

In the following we show how GW processes affect the tides and planetary waves as enumerated in Fig. 2, and we present numerical experiments that provide understanding.

2. Diurnal Tides

Generated primarily by solar heating, the dominant diurnal tides propagate with the Sun westward and are referred to as migrating tides. The non-migrating tides, not propagating with the Sun, are generated in the NSM with planetary waves (PW) -- and they are later discussed. Here we deal primarily with migrating tides, but the oscillations include also non-migrating components.

The basic effect of GW momentum deposition on the fundamental 24-hour diurnal tide is demonstrated in numerical results taken from Mayr et al. (1998). Fig. 3 shows the amplitude and phase of the meridional winds, generated with zonal wave number m = 1. Computer solutions are presented with (a) and without (b) GW source. The differences are small below about 60 km. But at higher altitudes, the GW increase the amplitudes of the tide and reduce its vertical wavelengths -- as illustrated in Fig. 4.

With Hines' GW parameterization, the waves amplify the tides, as shown by McLandress (1997b). Due to the nonlinear positive feedback associated with critical level absorption, the GW deposit momentum in vertical wind shears (e.g., Walterscheid, 1981). This is evident in Fig. 6 of MMCH, which describes the momentum source that generates the QBO. The kind of wave interaction required to produce the QBO is amplifying the diurnal tide.

2.1. Seasonal Variations with Planetary Wave Modulation

Satellite measurements show that the diurnal tide (DT) in the upper mesosphere exhibits large seasonal variations with peak amplitudes near equinox (Hays et al., 1994; Burrage et al., 1995a, b; McLandress et al., 1996; Huang and Reber, 2003). The observations are reproduced in the NSM (Mayr et al., 1998, 1999), which describes the DT and the zonal-mean variations, including QBO and SAO, generated with GW interactions. This is shown in Fig. 5, where we present numerical results for the zonal-mean winds (a) and the meridional wind amplitude of the tide (b). The DT in Fig. 5b is shown at 95 km and 18° latitude where the meridional winds peak. The mean zonal winds in Fig. 5a at 50 km are eastward in winter and westward in summer due to solar heating, and at 80 km the winds reverse direction due to GW filtering, as discussed in MMCH.

Our model results in Fig. 5 show that the peak amplitudes of the tide occur where the zonal winds change direction, which indicates that GW filtering is involved. The upward propagating GW interact with the large zonal winds during summer and winter months, and deposit momentum. Less GW momentum is thus available to amplify the tide around solstice (January/July), which could produce the amplitude maxima during equinox that are observed.

As Fig. 2 illustrates, the dynamical situation is more complicated than suggested and portrayed in Fig. 5. Numerous studies have shown (e.g., Lindzen and Hong, 1974; Forbes and Hagan, 1988; Hagan et al., 1993) that the zonal mean temperature and wind fields affect the diurnal tides and their seasonal variations. Moreover, the seasonal variations of the planetary waves (PW) absorb and in turn modulate the GW, which contributes to the variability of the tides. GW filtering by the diurnal and semi-diurnal tides can produce interactions that affect their seasonal variations. Mayr et al. (2001) discussed numerical experiments that describe these processes, and in the following we present some model simulations from that study.

The numerical results in Fig. 6 show the amplitude and phase of the diurnal tide (DT) at 95 km and 18° latitude. The standard solution (solid line, large + marks) accounts for all dynamical interactions between tides, PW, and zonal mean variations under the influence of GW. For comparison, a numerical experiment is presented (dotted lines, small + marks), in which the GW are turned off, but only for the tides and PW ($m > 0$). In this case, the GW still influence the DT through the zonal-mean wind and temperature variations -- and that interaction produces seasonal variations with equinoctial maxima (dotted lines). With GW source (solid lines), however, the equinoctial maxima are much more pronounced, and the phase is shifted to earlier local times. The interaction of the DT with the zonal mean circulation contributes to the semi-annual seasonal variations, shown by McLandress (1997a), but GW filtering is more important.

As shown in Section 5, the planetary waves (PW) are generated in the NSM internally by baroclinic instabilities, which can develop in the zonal-mean temperature variations, as proposed by Plumb (1983) and Pfister (1985) and confirmed in modeling studies (e.g., Norton and Thuburn, 1996, 1999). Fig. 7 shows the PW for $m = 3$ at 80 km, computed with and without GW interaction. The PW appear primarily around summer/winter solstice where instabilities develop. And the waves are greatly amplified by GW, which explains the enhanced PW modulation of the DT in Fig. 6.

The PW also affect the seasonal variation of the DT. This is shown in Fig. 7b, where we present the 5-day mean of the meridional wind amplitudes for the tide at 95 km, computed with and without the PW for $m = 3$ and 4. Without PW, the DT is much larger during summer months. This indicates that GW filtering by the PW is involved. The GW momentum expended to amplify the PW is not available to amplify the DT at higher altitudes.

The semi-diurnal tide (SDT) peaks at mid latitudes, and in Fig. 8a we present the computed zonal wind amplitudes at 95 km that are produced with and without GW. With the GW source, the PW modulations are large and similar to those of the DT in Fig. 6. The amplitude of the SDT is amplified by GW, and it peaks during winter and summer months when the DT is weakest. This relationship between the tides is made evident in Fig. 8b, where we present the 5-day mean of the SDT computed with and without the excitation of the DT. Without the DT, the amplitude of the SDT tends to be larger, and the differences are largest during the spring and fall seasons. Around equinox, the GW apparently amplify the DT at the expense of the SDT. (Without GW forcing, Mayr et al., 2001 report that the SDT is not much affected by the absence of the DT).

2.2. QBO-generated Inter-annual Variations

Satellite and ground-based measurements show that the diurnal tide (DT) reveals relatively large inter-annual variations in the upper mesosphere (e.g., Burrage et al., 1995a; Lieberman, 1997; Vincent et al., 1998). Hagan et al. (1999a) carried out an analysis with the Global Scale Wave Model (GSWM) and showed that the seasonal variations of the DT are significantly affected by linearized advection associated with the mean ($m = 0$) zonal winds. Advection produced with the observed QBO, however, could not reproduce the inter-annual variations of the DT (Hagan et al., 1999b). Applying Hines GW parameterization, McLandress (2002c) generated an 18-month QBO with zonal winds close to 40 m/s at 30 km. His analysis demonstrated that significant inter-annual variations were produced by the advection term from the meridional gradient of the QBO mean zonal winds.

The numerical results presented here are taken from Mayr and Mengel (2005). Fig. 9 shows the computed stratospheric QBO, and the inter-annual variations of the DT in the upper mesosphere. Near the equator, the zonal-mean ($m = 0$) zonal winds at 30 km (Fig. 9a) vary with a period close to 24 months, and that periodicity is evident in the amplitude of the DT at 95 km (Figs. 9b, c). A pronounced signature of inter-annual variations is also seen in the DT at 18° latitude (Fig. 9d), where amplitude maxima develop during the spring/fall seasons as observed and discussed in Section 2.1. The relationship between the stratospheric QBO and inter-annual variation of the DT is clearly evident, and the question is what are the mechanisms that produce this connection.

In agreement with Hagan et al. (1999a, b) and McLandress (2002c), our analysis with the NSM confirms the importance of advection for the inter-annual variation of the diurnal tide. But it also shows that the QBO-modulated GW momentum source dominates in the upper mesosphere.

The NSM is nonlinear, and we present here the linearized advection terms for the meridional and vertical components of the DT,

$$\langle v \rangle \frac{\partial U}{r \partial \theta} + \langle w \rangle \frac{\partial U}{\partial r} \qquad (1)$$

where U is the mean (m = 0) QBO zonal wind; $\langle v \rangle$, $\langle w \rangle$ represent the time-average amplitude of the meridional and vertical winds of the DT, respectively; and r, θ are Earth radius and latitude. (The zonal advection term can be ignored.)

The numerical results for advection are shown in Fig. 10. For the mean zonal winds, a 1-year running mean was taken to describe the QBO variability, and the terms were normalized to represent % variations in relation to the acceleration of the tide. Since meridional advection (Fig. 10a) becomes important away from the equator, the term is presented at 18° latitude where the DT peaks. The vertical advection (Fig. 10b) is shown at 4° near the equator, where the QBO zonal winds peak. Comparable in magnitude, the meridional and vertical advection terms reveal pronounced QBO like modulations around 30% in the stratosphere. But in the mesosphere above 60 km, the 24-month QBO signatures almost disappear. With QBO zonal winds of 20 m/s in the lower stratosphere, the advection terms cannot reproduce the inter-annual variations of the tide that are generated with the NSM.

In the upper mesosphere, GW become important. This is shown in Fig. 11, where we present the QBO zonal winds (a), the GW momentum source (b), and the variability of the tide at 95 km (c). For the amplitudes of the GW source (Fig. 11b), the normalized relative variations (%) are presented, analogous to Fig. 10. Above 80 km, year-to-year variations of about 20% are generated, and the period is close to 24 months of the QBO. The yearly variation of the DT (Fig. 11c) shows amplitude maxima and minima that are aligned with the GW source (Fig. 11b), which demonstrates that the GW modulate the tide. The GW are apparently filtered by the QBO zonal winds in the middle atmosphere. During the years 3, 5, 7, the waves appear to be preferentially absorbed, and the resulting momentum deficits reduce the amplitudes of the DT at higher altitudes.

In the stratosphere, the momentum advection from the QBO zonal winds is very effective in modulating the tide. But in the mesosphere, the GW filtered by the QBO attain large amplitudes and provide the momentum source that generates the inter-annual variations.

3. Non-migrating Tides

The so-called diurnal and semi-diurnal migrating tides (MT) propagate westward with the Sun, occupy m = 1 and 2, and have periods of 24 and 12 hours, respectively. The non-migrating tides (NMT) also have periods of 24 and 12 hours, commensurate with solar heating. But unlike the MT, the NMT can propagate eastward, be stationary (m = 0), or occupy any wave number.

NMT have been observed in the middle atmosphere with satellite borne wind and temperature measurements (e.g., Lieberman, 1991; Forbes et al., 1995, 2003; Talaat and Lieberman, 1999; Oberheid et al., 2002; Huang and Reber, 2004). The observed phase structure of the NMT indicates that the tides propagate upward (e.g., Lieberman. 1991; Talaat and Lieberman, 1999).

Hagan and Forbes (2003) demonstrated that NMT can be generated by topography and latent heat release associated with convection. They showed that this tropospheric source contributes significantly to the observed tidal amplitudes in the upper mesosphere.

Teitelbaum and Vial (1991) proposed that nonlinear coupling between migrating tides (MT) and planetary waves (PW) can generate NMT. Observed correlations between MT and PW activity provide observational evidence for this mechanism (e.g., Forbes et al., 1995; Talaat and Lieberman,

1999, Pancheva et al., 2002); and modeling studies have shown that the interaction can produce NMT with large amplitudes (e.g., Miyahara et al., 1997, 1999; Hagan and Roble, 2001, Coll and Forbes, 2002).

The NSM generates the NMT with PW (Mayr et al., 3003, 2005a, b), and Fig. 12 presents the meridional wind amplitudes for the 24-hour tides at 100 km. As discussed in Section 2.1, the dominant diurnal westward propagating MT with m = 1 peaks near 20° latitude (Fig. 12a). The amplitudes are largest (~ 100 m/s) during the spring and fall seasons, owing in part to GW filtering by the mean zonal winds. The m = 1 eastward propagating NMT (Fig. 13b) is highly variable, and it peaks around the equator with velocities between 10 and 30 m/s. Similar amplitudes are also generated in the stationary NMT (m = 0) shown in Fig. 12c.

The mechanism for generating NMT with PW is illustrated in Fig. 13. Numerical results are presented for the stationary m = 0 NMT, which is produced through non-linear interactions between PW and the diurnal MT, each having wave number m = 1. Fig. 13a represents the standard solution for the meridional wind amplitude of the NMT and the zonal wind PW at 100 km and 18° latitude. During the initial 6 months of the model run, the amplitudes are relatively small. But later, the PW and NMT attain values that approach 20 and 40 m/s respectively. The amplitude variations show evidence of correlations. For comparison, we present in Fig. 13b numerical results from a model run without the zonal-mean heat source that produces the PW through instabilities. After the initial start-up noise, the PW and NMT are no longer generated.

The NSM is fully nonlinear, and a number of processes could produce the interaction between PW and MT that generates the NMT (Figs. 12 and 13). Gravity wave (GW) filtering can also produce nonlinear interactions, as shown for example in MMCH for the 5-year oscillation, and in Sections 2.2 for the inter-annual variations of the diurnal tide. For the NMT, the proposed nonlinear GW interaction is illustrated in Fig. 14. Upward propagating GW encounter a long-period PW and deposit eastward momentum in the eastward phase of the wind oscillation. The wave momentum given to the PW is then missing in the GW when they encounter the MT at higher altitudes. Since the GW amplify the tide, its eastward (positive) phase is weaker than the westward phase. And GW filtering by the negative phase of the PW produces the weaker negative phase of the tide. In effect, the tide is modulated by PW, which is a signature of nonlinear interaction.

Fig. 15 is taken from Mayr et al. (2005b) and presents numerical results for the m = 0 NMT from solutions with and without GW source, which indicates that the waves contribute significantly to the nonlinear coupling between MT and PW. In this study, the GW source was simply turned off after 5 years, and the subsequent 3 months are shown for the meridional and zonal winds at 100 km. Having integrated the model sufficiently long, the idea was that the inertia in the zonal-mean temperature and wind velocity could maintain, for a limited time, the PW and MT at full strengths. For the PW, our numerical results confirm that. But for the MT involved, the zonal and meridional winds vary in opposite directions when the GW source is turned off. The large differences apparent in Fig. 15 thus must be taken with some caution.

A more definitive demonstration of the GW process is presented in Fig. 16, taken from Mayr et al. (2003, 2005b). The focus here is the nonlinear GW interaction specifically, which is involved in generating the m = 0 NMT. The model was run for perpetual equinox, without time dependent solar heating. For comparison, the model was then integrated again but with a GW momentum source for m = 0 that was forced to remain constant after 18 months. In this control experiment, only the non-linear GW interaction is suppressed that can generate the NMT. All the other GW processes are retained that filter the MT and produce the PW through instabilities. The building blocks of the NMT are generated without interference.

Fig. 16a shows the computed meridional wind amplitude of the westward propagating m = 1 diurnal tide at 100 km. Both solutions are presented, and the differences are small. For the m = 1 PW in Fig. 16b, the time independent GW source produces somewhat larger velocities. Fig. 16c then

shows the m = 0 non-migrating diurnal tide computed with and without the time independent GW momentum source, and the differences are large after 18 months. Without the GW interaction (lower panel), the NMT is greatly reduced, although the PW involved are somewhat stronger (Fig. 16b). This clearly demonstrates that the GW contribute significantly to the nonlinear coupling between MT and PW.

4. Planetary-scale Inertio Gravity Waves

In the upper mesosphere, oscillations with periods around 10 hours have been observed with different measurement techniques. Analyzing radar wind measurement at Saskatoon (52° N), Manson et al. (1982) and Manson and Meek (1990) discovered persistent oscillations with periods of 9-10 and 16 hours, which were attributed to nonlinear coupling between the semidiurnal tide and planetary waves. Similar kind of variations were also reported by Ruster (1994) and Sivjee et al. (1994). In optical measurements of winds and temperatures at 90 km, Hernadez et al. (1992, 1993) observed pronounced westward propagating waves with a period of 10.1 hours near the South Pole. The inferred large vertical wavelength indicated that a Lamb wave was observed. At the South Pole (88° S), westward propagating wind oscillations with periods 7 - 12 hours were observed with radar measurements (Forbes et al., 1999; Portnyagin et al., 2000). Lamb waves and "normal modes" were invoked, but inertio gravity waves, nonlinear coupling between tides and planetary waves were also suggested as possible explanations. With measurements from a number of instruments at northern high latitudes, Wu et al. (2002) observed 10-hour oscillations in the temperature and wind fields of the upper mesosphere and lower thermosphere. A zonal wave number m = 5 was inferred, and the vertical wavelength was estimated at 53 km. The authors proposed that the oscillations could be generated by the nonlinear interaction between the semidiurnal tide and 2-day planetary waves.

The NSM generates in the upper mesosphere oscillations with periods around 10 hours having zonal wave numbers m = 0 - 2 (Mayr et al., 2003, 2004). In Fig. 17, the computed meridional wind (a) and temperature (c) variations are shown at 84° N for a short time span in March of the third model year when the oscillations are relatively large. Like diurnal tides, the waves propagate upward, increase in amplitude, and the vertical wavelengths are around 20 km. The winds and temperature perturbations attain at 100 km values close to 20 m/s (Fig. 17a) and 5 K (Fig. 17c), respectively. The power spectrum for the meridional winds (Fig. 17b), obtained from a time span of 20 days, shows that the amplitudes for the 9 and 10-hour waves exceed those of the non-migrating 12-hour semidiurnal tide. As was shown for the diurnal tides, the large wave amplitudes in the mesosphere are presumably produced in part by GW momentum deposition due to critical level absorption in vertical wind shears.

In our model results, the temperature oscillations for m = 0 tend to peak at the poles. The m = 1 horizontal winds can also peak at the poles, but that depends on the direction of propagation as shown in Fig. 18. Presented here are the meridional wind spectra at 100 km obtained from a 6-month time span following December solstice. With a running window of 15 days, the westward (red) and eastward (blue) propagating waves were derived. As expected, the westward propagating 12-hour semidiurnal tide dominates, which attains peak amplitudes close to 40 m/s near the poles in both hemispheres. The spectra also show pronounced amplitudes for oscillations with periods close to 10 and 9 hours, which propagate westward and reach amplitudes exceeding 20 m/s near the North Pole. The weaker eastward propagating waves have amplitudes ~ 10 m/s, confined to mid latitudes.

The dynamical conditions characterizing these oscillations have much in common with the earlier discussed diurnal tides. With periods close to 12 hours, the Coriolis force is important; the vertical wavelengths have similar magnitudes; and the oscillations have low zonal wave numbers (m < 4). Based on classical tidal theory (Longuett-Higgins, 1968), close examination shows that the oscillations are related to Class-1 waves or Hough modes, which have also been referred to as Inertio Gravity Waves (Andrews et al., 1987; Volland, 1988). Since the waves occupy low zonal wave numbers, we

refer to them as Planetary-scale Inertio Gravity Waves (PIGW). The PIGW differ from typical Inertio Gravity Waves (IGW), which have also periods between 5 and 11 hours but are observed with much shorter horizontal wavelengths from 500 to 3000 km (Fritts, 1984; Fritts et al., 1984; Muraoka et al., 1988; 1994; Tsuda et al., 1989).

With relatively long horizontal wavelengths and short oscillation periods, the PIWG in our model have phase velocities in excess of the background zonal winds. Unlike the slower planetary waves (PW) with longer periods, or IGW with shorter wavelengths, the fast PIGW can propagate through the atmosphere without dissipation due to critical level absorption.

The seasonal variations of the PIGW are shown in Fig. 19a for the m = 1 meridional winds at 100 km. In both hemispheres, the waves are generated preferentially around winter solstice, extending into spring. Consistent with Fig. 18, the westward and eastward propagating oscillations are respectively confined to high and mid latitudes. Our analysis shows that the waves are not generated when the zonal-mean heat source of the atmosphere is turned off. Like the PW, later discussed, the PIGW are in part generated by instabilities.

The diurnal tides are also involved. And this is shown in Fig. 18b, where we present the m = 1 PIGW computed without the excitation of the migrating diurnal tides. The amplitudes are of comparable magnitudes, but the seasonal variations differ considerably. The PIGW in Fig. 18a are apparently generated like the non-migrating tides through nonlinear coupling between PW and migrating tides, as had been suggested in several papers (e.g., Manson et al., 1982; Manson and Meek, 1990; Forbes et al., 1999; Portnyagin et al., 2000).

In light of the results shown in Fig. 18b, it is not surprising that 12-hour pseudo tides are generated without the solar excitation of migrating tides (Talaat and Mayr, 2010). In the upper mesosphere, and in the NSM, this class of non-migrating tides contributes significantly to the semi-diurnal oscillations at high latitudes.

5. Planetary Waves

The dynamical properties of planetary waves (PW) are well understood and have been discussed in the textbook literature (e.g., Holton 1979; Volland, 1988). Topographic forcing and tropical convection can produce the PW originating in the troposphere, and the baroclinic instability has been invoked for the PW generated in the mesosphere (Plumb, 1983; Pfister, 1985). As the PW propagate through the middle atmosphere, they attain large amplitudes in the upper mesosphere as observed with ground-based and spacecraft measurements (e.g., Muller and Nelson, 1978; Craig and Elford, 1981; Burks and Leovy, 1986; Tsuda et al., 1988; Phillips, 1989; Poole, 1990; Wu et al., 1993; Fraser et al., 1993; Clark et al., 1994; Fritts and Isler, 1994; Harris, 1994; Smith, 1996; 1997; Meek et al., 1996; Deng et al., 1997; Fritts et al., 1999; Talaat and Lieberman, 1999; Wang et al., 2000; Talaat et al., 2001).

In the NSM, the PW are generated internally by instabilities associated with the zonal-mean variations of temperature, density, and zonal winds. As shown in Fig. 13, the PW are not excited when the zonal-mean heating is turned off. The model does not describe the PW that are produced in GCMs by topography and tropical convection (e.g., Giorgetta et al., 2002; Horinouchi et al., 2003).

The zonal-mean (m = 0) temperature variations in the NSM are presented in Fig. 20a for December solstice, and Fig. 20b illustrates the associated dynamical processes. Owing to solar heating in the stratosphere and lower mesosphere, the temperatures decrease in winter and increase in summer to produce respectively eastward (positive) and westward (negative) zonal winds. Generated by GW interaction with the zonal circulation (Lindzen, 1981), the zonal winds reverse direction in the mesosphere, and in geostrophic balance the temperatures turn colder in summer than in winter. Due to GW, the meridional circulation in the mesosphere increases to such magnitude that more energy is removed in summer than provided by solar radiation.

Around the tropopause, cumulus heating at low latitudes is generating zonal jets that are observed at mid latitudes. This is simulated in the NSM with a time independent tropospheric zonal-mean heat source. The heat source generates in the model the temperature variations in Fig. 20, which peak at the equator in the troposphere but increase to higher latitudes in the lower stratosphere, in qualitative agreement with observations.

The dynamical conditions in the troposphere are to some extent similar to those occurring in middle atmosphere, as illustrated in Fig. 20b. In the mesosphere, GW filtering causes the zonal winds and temperature variations to reverse at higher altitudes, which is conducive for generating PW through baroclinic instabilities (Plumb, 1983). We believe that GW interactions could also produce the reversing temperature variations around the tropopause, to generate, in the NSM, the tropospheric PW through instabilities.

In Fig. 21, we present at mid latitudes the PW for m = 1 and 3 at 90 km, which are generated with (a) and without (b) the tropospheric heat source. With the tropospheric source, the long-period PW amplitudes for m = 1 are highly variable but tend to peak during the spring and fall seasons. Without the source, the oscillations are greatly reduced and much less variable; and the differences for the m = 2 PW show similar patterns. For the PW with m = 3, the tropospheric source also increases the wave amplitudes but mainly in winter and around equinox. These short-period waves are generated mainly in the stratosphere and mesosphere.

The seasonal/latitudinal variations of the m = 3 PW are shown in Fig. 22 at 60 and 90 km. The amplitudes are computed with running windows, in which the oscillation periods are multiplied by a factor of 3. (Individual wave amplitudes are considerably larger.) Fig. 22a shows at 60 km that the oscillations extend from the equator to high latitudes and occupy primarily the winter hemisphere. At 90 km (Fig. 22b), however, the pattern is markedly different. The oscillations populate the region around the equator and extend at higher latitudes into the summer hemisphere. At both altitudes, the amplitudes approach values close to 30 m/s.

Our analysis indicates that the changes in the seasonal pattern of the m = 3 PW, also seen in m = 4, are produced by variations in the baroclinic instabilities that prevail in the stratosphere and mesosphere. This is shown in Fig. 23, where we present at 50 and 90 km the normalized differences between the relative latitudinal pressure and density gradients for the zonal mean (m = 0). The gradients are largest at 50 km in winter (Fig. 23a), but at 90 km in summer (Fig. 23b). In the mesosphere, the reversal of the latitudinal temperature variations (Fig. 20) is accompanied by changing baroclinicity, which in turn produces the changes in the seasonal PW pattern in Fig. 22.

6. Summary

We summarize numerical results from the Numerical Spectral Model (NSM). The model is integrated from the ground into the thermosphere, and it is fully non-linear. The spectral formulation allows us to analyze the individual, and interacting, dynamical components with different zonal wave numbers, which describe the zonal-mean variations, tides, and planetary waves.

The NSM employs the Doppler Spread Parameterization (DSP) for small-scale gravity waves (GW) developed by Hines (1997a, b). This formulation reproduces a broad range of dynamical features observed in the zonal-mean (HMCF) -- in particular the quasi-biennial oscillation (QBO) of the stratospheric circulation, which is generated with GW momentum deposition owing to critical level absorption.

The kind of GW source that generates the QBO can also amplify the tides (Walterscheid, 19861). This is shown in the present paper with numerical results, which demonstrate that the GW amplify the tides and planetary waves, and presumably the planetary-scale inertio gravity waves and related pseudo tides.

In Hines' GW parameterization, the wave momentum flux is conserved, which has important consequences. The GW momentum source that generates the QBO is not available to amplify the tides at higher altitudes. Through GW filtering, the QBO signature is transferred to the diurnal tide to generate inter-annual variations in the upper mesosphere. The GW momentum, expended in the annual variations of the mean zonal winds, produces equinoctial amplitude maxima in the diurnal tide. And GW interactions with the diurnal tide significantly affect the seasonal variations of the semi-diurnal tide. Numerical experiments demonstrate that GW produce nonlinear interactions between migrating tides and planetary waves, to generate non-migrating tides.

As the GW propagate up through the atmosphere, they carry the accumulating imprints of interactions with the zonal-mean variations, tides, and planetary waves. The accompanying nonlinear interactions, due to GW filtering and momentum deposition, produces a climatology that becomes increasingly more complex at higher altitudes -- apparent in our model results and in qualitative agreement with observations.

References

Akmaev, R.A., Forbes, J.M., Hagan, M.E., 1996. Simulation of tides with a spectral mesosphere/lower thermosphere model, Geophys. Res. Lett., 23, 2173.

Akmaev, R.A., 2001a. Simulation of large-scale dynamics in the mesosphere and lower thermosphere with the Doppler-spread parameterization of gravity waves: 1. Implementation and zonal mean climatology, J. Geophys. Res., 106, 1193.

Akmaev, R.A., 2001b. Simulation of large-scale dynamics in the mesosphere and lower thermosphere with the Doppler-spread parameterization of gravity waves: 2. Eddy mixing and diurnal tide, J. Geophys. Res., 106, 1205-1213.

Andrews, D.G., Holton, J.R., Leovy, C.B., 1987. Middle Atmosphere Dynamics, Academic Press, Orlando, 1987.

Avery, S.K., Vincent, R.A., Phillips, A., Manson, A.H., Fraser, G.R., 1989. High latitude tidal behavior in the mesosphere and lower thermosphere, J. Atm. Terr. Phys., 51, 595.

Burks, D., Leovy, C., 1986. Planetary waves near the mesospheric easterly jet, Geophys. Res. Lett., 13, 193.

Burrage, M.D., Hagan, M.E., Skinner, W.R., Wu, D.L., Hays, P.B., 1995a. Long-term variability in the solar diurnal tide observed by HRDI and simulated by the GSWM, Geophys. Res. Lett., 22, 2641.

Burrage, M.D., Wu, D.L., Skinner, W.R., Ortland, D.A., Hays, P.B., 1995b. Latitude and seasonal dependence of the semidiurnal tide observed by the high-resolution Doppler imager, J. Geophys. Res., 100, 11313.

Chan, K.L., Mayr, H.G., Mengel, J.G., Harris, I., 1994. A 'stratified' spectral model for stable and convective atmospheres, J. Comp. Phys., 113, 165.

Chan, K.L., Mayr, H.G., Mengel, J.G., Harris, I., 1995. A numerical spectral model for the mean zonal circulation and the tides in the middle and upper atmosphere, Geophys. Monogr., 87, 265.

Chapman, S., Lindzen, R.S., 1970. Atmospheric Tides, D. Reidel, Hingham, MA, 1970.

Clark, R.R., Current, A.C., Manson, A.H., et al., 1994. Global properties of the 2-day wave from mesosphere lower-thermosphere radar observations, J. Atmos. Terr. Phys., 56, 1279.

Coll, M.A.I., Forbes, J.M., 2002. Nonlinear interactions in the upper atmosphere: The s = 1 and s = 3 non-migrating semidiurnal tides, J. Geophys. Res., 107, 1157.

Craig, R.L., Elford, W.G., 1981. Observations of the quasi 2-day wave near 90 km altitude at Adelaide (33° S), J. Atmos. Terr. Phys., 43, 1051.

Deng, W., Salah, J.E., Clark, R.R., et al., 1997. Coordinated global radar observations of tidal and planetary waves in the mesosphere and lower thermosphere during January 20-30, 1993, J. Geophys. Res., 102, 7307.

Forbes, J.M., Hagan, M.E., 1988. Diurnal propagating tides in the presence of mean winds and dissipation: a numerical investigation, Planet. Space Sci., 36, 579.

Forbes, J.M., Gu, M.J., Miyahara, S., 1991. On the interaction between gravity waves and the diurnal propagating tide, Planet. Space Sci., 39, 1249.

Forbes, J.M., Vial, F., 1989. Monthly simulations of semidiurnal tide in the mesosphere and lower thermosphere, J. Atm. Terr. Phys., 51, 649.

Forbes, J.M., Makarov, N.A., Portnyagin, Y.I., 1995. First results from the meteor radar at South Pole: A large 12-hour oscillation with zonal wave number one, Geophys. Res. Lett., 22, 3247.

Forbes, J.M., and Garrett, H.B., 1978. Thermal excitation of atmospheric tides due to insolation absorption by O_3 and H_2O, Geophys. Res. Lett., 5, 1013.

Forbes, J.M., 1995. Tidal and planetary waves, Geophys. Monogr. 87, 67.

Forbes, J.M., Palo, S.E., Zhang, X., Portnyagin, Y.I., Makarov, N.A., Merzlyakov, E.G., 1999. Lamb waves in the lower thermosphere: Observational evidence and global consequences, J. Geophys. Res., 104, 17107.
Forbes, J.M., Guffee, R., Zhang, X., Riggin, M.D., Marsh, D.R., et al., 1997. Quasi 2-day oscillation of the ionosphere during summer 1992, J. Geophys. Res., 102, 7301.
Forbes, J.M., Hagan, M.E., Miyahara, S., Miyoshi, Y., Zhang, X., 2003. Diurnal non-migrating tides in the tropical lower thermosphere, Earth, Plan. Space, 55, 419.
Fraser, G.J., Hernadez, G., Smith, R.W., 1993. Eastward moving 2-4 day waves in the winter Antarctic mesosphere, Geophys. Res. Lett., 20, 1547.
Fritts, D.C, 1984. Gravity wave saturation in the middle atmosphere: A review of theory and observations, Rev. Geophys. Space Phys., 22, 275
Fritts, D.C., 1995a. Gravity wave-tidal interactions in the middle atmosphere: observations and theory, Geophys. Monogr. 87, 89.
Fritts, D.C., 1995b. Gravity wave forcing and effects in the mesosphere and lower thermosphere, Geophys. Monogr. 87, 121.
Fritts, D.C., Balsley, B.B., Ecklund, W.L., 1984. VHF echoes from the arctic mesosphere and lower thermosphere, Part II: Interpretations, in Dynamics of the Middle Atmosphere, Eds., J. R. Holton and T. Matsuno, 97.
Fritts, D.C., Vincent, R.A., 1987. Mesospheric momentum flux studies at Alelaide, Australia: Observations and a gravity wave tidal interaction model, J. Atmos. Sci., 44, 605.
Fritts, D.C., Isler, J.R., 1994. Mean motion and tidal and 2-day structure and variability in the mesosphere and lower thermosphere, J. Atmos. Sci., 51, 2145.
Fritts, D.C., Isler, J.R., Lieberman, R.S. et al., 1999. Two-day wave structure and mean flow interactions observed by radar and High Resolution Doppler Imager, J. Geophys. Res., 104, 3953.
Geller, M.A., Yudin V.A., Khattatov, B.V., Hagan M.E., 1997. Modeling the diurnal tide with dissipation derived from UARS/HRDI measurements, Ann. Geophys., 15, 1198.
Gille, S.T, Hauchacorne, A., Chanin, M.L., 1991. Semidiurnal and diurnal tidal effects in the middle atmosphere as seen by Rayleigh lidar, J. Geophys. Res., 96, 7579.
Giorgetta, M.A., Mancini, E., Roeckner, E., 2002: Forcing of the quasi-biennial oscillation from a broad spectrum of atmospheric waves, J. Atmos. Sci., 54, 883.
Hagan. M.E., 1996. Comparative effects of migrating solar sources on tidal signatures in the middle and upper atmosphere, J. Geophys. Res., 101, 21213.
Hagan, M.E., Chang, J.L., Avery, S.K., 1997. Global-scale wave model estimates of non-migrating tidal effects, J. Geophys. Res., 102, 163493.
Hagan, M.E., Burrage M.D., Forbes J.M., Hackney, J., Randel, W.J., Zhang, X., 1999a. GSWM-98: Results for migrating solar tides, J. Geophys. Res., 104, 6813.
Hagan, M.E., Burrage M.D., Forbes J.M., Hackney, J., Randel, W.J., Zhang, X., 1999b. QBO effects in the diurnal tide in the upper atmosphere, Earth Planets Science, 51, 571,
Hagan, M.E. Roble, R.G., 2001. Modeling diurnal tidal variability with the National Center for Atmospheric Research thermosphere-ionosphere-mesosphere-electrodynamics general circulation model, J. Geophys. Res., 106, 24,869-24,882.
Hagan, M.E., Forbes, J.M., Vial, F., 1993. On modeling migrating solar tides, Geophys. Res. Lett., 22, 893.
Hagan, M.E., Forbes, J. M., 2002. Migrating and non-migrating semidiurnal tides in the upper atmosphere excited by tropospheric latent heat release, J. Geophys. Res., 108.
Harris, T.J., 1994. A long-term study of the quasi 2-day wave in the middle atmosphere, J. Atm. Terr. Phys., 56, 569.
Hays, P.B., Wu, D.L., and the HRDI science team, 1994. Observations of the diurnal tide from space, J. Atmos. Sci., 51, 3077.

Hernandez, G., Smith, R.W., Fraser, G.J., Jones, W.L., 1992. Large-scale waves in the upper mesosphere at Antarctic high-latitudes, Geophys. Res. Lett., 19, 1347, 1992.
Hernandez, G., Fraser, R.W., Smith, G. J., 1993. Mesospheric 12-hour oscillation near south pole Antarctica, Geophys. Res. Lett., 20, 1787, 1993.
Hines, C.O., 1997a. Doppler-spread parameterization of gravity-wave momentum deposition in the middle atmosphere, 1, Basic formulation, J. Atmos. Solar Terr. Phys., 59, 371.
Hines, C.O., 1997b. Doppler-spread parameterization of gravity-wave momentum deposition in the middle atmosphere, 2, Broad and quasi monochromatic spectra, and implementation, J. Atmos. Solar Terr. Phys., 59, 387.
Holton, J.R., 1979. An Introduction to Dynamic Meteorology, Academic Press.
Holton, J.R., 1984. The generation of mesospheric planetary waves by zonally asymmetric gravity wave breaking, J. Atmos. Sci., 41, 3427.
Horinouchi, T. et al., 2003. Tropical cumulus convection and upward propagating waves in middle atmospheric GCMs, J. Atmos. Sci., 60, 2765
Huang, F.T., Reber, C.A., 2003. Seasonal behavior of the semidiurnal and diurnal tides and mean flows at 95 km based on measurements from the High Resolution Doppler Imager (HRDI) on the Upper Atmospheric Research Satellite (UARS), J. Geophys. Res., 108.
Huang, F.T., Reber, C.A., 2004. Non-migrating semidiurnal and diurnal tides at 95 km based on wind measurements from the High Resolution Doppler Imager (HRDI) on UARS, J. Geophys. Res., 109.
Huang, F.T., et al., 2006. Diurnal variations of temperature and winds inferred from TIMED and UARS measurements, J. Geophys. Res., 111, A10S04, doi:1029/2009JD013698.
Huang, F.T., et al., 2010. Temperature diurnal variations (migrating tides) in the stratosphere and lower mesosphere based on measurements from SABER on TIMED, J. Geophys. Res., 115, D10111, doi:1029/2005JA011426.
Kato, S., 1980. Dynamics of the Upper Atmosphere, D. Reidel, Dordrecht.
Leblanc, T., McDermid, L.S., Ortland, D.A., 1999a. Lidar observations of the middle atmospheric thermal tides and comparison with the High-resolution Doppler Imager and Global Scale Model. 1. Methodology and winter observations at Table Mountain (34.4°N), J. Geophys. Res., 104, 11917.
Leblanc, T., McDermid, L.S., Ortland, D.A., 1999b. Lidar observations of the middle atmospheric thermal tides and comparison with the High-resolution Doppler Imager and Global Scale Model. 2. October observations at Mauna Loa (19.5° N), J. Geophys. Res., 104, 11931.
Lieberman, R., 1991. Nonmigrating diurnal tides in the equatorial middle atmosphere, J. Atmos. Sci., 48, 1112.
Lieberman, R., 1997. Long-term variations of zonal mean winds and (1,1) driving in the equatorial lower thermosphere, J. Atm. Sol. Terr. Phys., 59, 1483.
Lindzen R.S., 1981. Turbulence and stress due to gravity wave and tidal breakdown, J. Geophys. Res., 86, 9707.
Lindzen, R.S., Hong, S., 1974. Effects of mean winds and horizontal temperature gradients on solar and lunar semidiurnal tides in the atmosphere, J. Atmos. Sci., 31, 1421.
Longuett-Higgins, M.S., 1968. The eigenfunctions of Laplace's tidal equations over a sphere, Phi. Trans. Roy. Soc. London, A262, 511.
Manson, A.H., Meek, C.E., Teitelbaum, H., Vial, F., Schminder, R., Kuerschner, D., Smith, M.J., Fraser, G.J., Clark, R.R., 1989. Climatology of semidiurnal and diurnal tides in the middle atmosphere (70-110 km) at middle latitudes (40-55°), J. Atm. Terr. Phys., 51, 579.
Manson, A.H., Meek, C.E., 1990. Long period (8-20h) wind oscillations in the middle atmosphere at Saskatoon (52° N): Evidence for nonlinear tidal effects, Plan. Space Sci., 38, 1431.

Manson, A.H., Meek, C.E., Gregory, J.B., Chakraparty, D.K., 1982. Fluctuations in the tidal (24, 12 h) characteristics and oscillations (8h-5h) in the mesosphere and lower thermosphere, Plan. Space Sci., 30, 1283.

Manson, A.H., Luo, Y., Meek, C., 2002. Global distribution of diurnal and semi-diurnal tides: observations from HRDI-UARS of the MLT region, Ann. Geophys., 20, 1877.

Mayr, H.G., Mengel, J.G., Chan, K.L., Porter, H.S., 1998. Seasonal variations of the diurnal tide induced by gravity wave filtering, Geophys. Res. Lett., 25, 943.

Mayr, H.G., Mengel, J.G., Chan, K.L., Porter, H.S., 1999. Seasonal variations and planetary wave modulation of diurnal tides influenced by gravity waves, Adv. Space Res., 24, 154.

Mayr, H.G., Mengel, J.G., Chan, K.L., Porter, H.S., 2001 Mesosphere dynamics with gravity wave forcing: Part I, Diurnal and semidiurnal tides, J. Atm. Solar-Terr. Phys., 63, 1851.

Mayr, H.G., Mengel, J.G., Talaat, E.R., Porter, H.S., Chan, K.L., 2003a. Non-migrating diurnal tides generated with planetary waves in the mesosphere, Geophys. Res. Lett., 30, 1832.

Mayr, H.G., Mengel, J.G., Talaat, E.R., Porter, H. S., Chan, K.L., 2003b. Planetary-scale inertio gravity waves in the mesosphere, Geophys. Res. Lett., 30, 2228.

Mayr, H.G., Mengel, J.G., Talaat, E.R., Porter, H. S., Chan, K.L., 2004a. Modeling study of atmospheric planetary waves: genesis and characteristics, Ann. Geophys., 22, 1885.

Mayr, H.G., Mengel, J.G., Talaat, E.R., Porter, H. S., Chan, K.L., 2004b. Properties of internal planetary-scale inertio gravity waves in the mesosphere, Ann. Geophys., 22, 3421.

Mayr, H.G., Mengel, 2005. Interannual variations of the diurnal tide in the mesosphere generated by the quasi-biennial oscillation, J. Geophys. Res., 110, D10111.

Mayr, H.G., Mengel, J.G., Talaat, E.R., Porter, H. S., Chan, K.L., 2005a. Mesospheric non-migrating tides generated with planetary waves: I. Characteristics, J. Atm. Solar Terr. Phys., 67, 959.

Mayr, H.G., Mengel, J.G., Talaat, E.R., Porter, H. S., Chan, K.L., 2005a. Mesospheric non-migrating tides generated with planetary waves: II. Influence of gravity waves, J. Atm. Solar Terr. Phys., 67, 981.

Mayr, H.G., Mengel, J.G., Chan, K.L., Huang, F.T., 2010. Middle atmosphere dynamics with gravity wave interactions in the numerical spectral model: Zonal mean variations, J. Atmos. Solar Terr. Phys., 72, 807.

McLandress, C., Shepherd, G.G., Solheim, B.H., 1996. Satellite observations of thermospheric tides: Results from the Wind Imaging Interferometer on UARS, J. Geophys. Res., 101, 4093.

McLandress, C., 1997a. Seasonal variability of the diurnal tide: Results from the Canadian Middle Atmosphere General Circulation Model, J. Geophys. Res., 102, 29747.

McLandress, C., 1997b. Sensitivity studies using the Hines and Fritts gravity wave drag parameterizations, NATO ASI Series, Vol. 150, 245.

McLandress, C., 2002a. The seasonal variation of the propagating diurnal tide in the mesosphere and lower thermosphere. Part I: The role of gravity waves and planetary waves, J. Atmos. Sci., 59, 5, 893.

McLandress, C., 2002b. The seasonal variation of the propagating diurnal tide in the mesosphere and lower thermosphere. Part II: The role of tidal heating and zonal mean winds, J. Atmos. Sci., 59, 5, 907.

McLandress, C., 2002c. Inter-annual variations of the diurnal tide in the mesosphere induced by a zonal-mean wind oscillation in the tropics, Geophys. Res. Lett., 29, 9, doi:10.1029/2001GL014551.

Mengel, J.G., Mayr, H.G., Chan, K.L., Hines, C.O., Reddy, C.A., Arnold, N.F., Porter, H.S., 1995. Equatorial oscillations in the middle atmosphere generated by small-scale gravity waves, Geophys. Res. Lett., 22, 3027.

Meek, C.E., Manson, A.H., Franke, S.J., Singer, W. et al., 1996. Global study of northern hemisphere quasi 2-day wave events in recent summers near 90 km altitude, J. Atm. Terr. Phys., 58, 1401.

Miyahara, S, Yoshida, Y., Miyoshi, Y., 1993. Dynamical coupling between the lower and upper atmosphere by tides and gravity waves, J. Atm. Terr. Phys., 55, 1039.
Miyahara, S., Miyoshi, Y, Yamashita, K., 1999. Variations of migrating and non-migrating atmospheric tides simulated by a middle atmosphere general circulation model, Adv. Space Res., 24(11), 1549-1558.
Miyahara, S., Forbes, J.M., 1991. Interaction between gravity waves and the diurnal tide in the mesosphere and lower thermosphere, J. Meteoor. Soc. Japan, 69, 523.
Muraoka, Y., Sugyama, T., Kawahira, K., 1988. Cause of a monochromatic inertio-gravity wave breaking observed by the MU radar, Geophys. Res. Lett., 15 , 1349, 1988.
Muraoka, Y, Fukao, S., Sugyama, T., Yamamoto, M., Nakamuro, N., Tsuda, T., Kato, S., 1994. Features of the mesospheric inertio-gravity waves observed with the MU radar, J. Atmos. Terr. Phys., 56, 1163.
Mukhtarov, P., Pancheva, D., Andonov, B., 2009. Global structure and seasonal and interannual variability of the migrating diurnal tide seen in SABER/TIMED temperatures between 20 and 120 km, J. Geophys. Res., 114, A02309, doi:10.1029/2008JA013759.
Muller, H.G., Nelson, L., 1978. A traveling quasi 2-day wave in the meteor region, J. Atm. Terr. Phys., 40, 761.
Norton, W.A., Thuburn, J., 1996. The two-day wave in a middle atmosphere GCM, Geophys. Res. Lett., 23, 2113.
Norton, W.A., Thuburn, J., 1999. Sensitivity of mesospheric mean flow, planetary waves and tides to strength of gravity wave drag, J. Geophys. Res., 104, 30,897, 1999.
Oberheide, J., Hagan, M.E., Roble, R.G., Offermann, D., 2002. Source of non-migrating tides in the tropical middle atmosphere, J. Geophys. Res., 107.
Pancheva, D et al., 2002. Global-scale tidal variability during the PSMOS campaign for June-August 1999: interaction with planetary waves, J. Atm. Solar Terr. Phys., 64, 1865.
Pfister, L., 1985. Baroclinic instability or easterly jets with application to the summer mesosphere, J. Atmos. Sci., 42, 313.
Phillips, A., 1989. Simultaneous observations of the quasi 2-day wave at Manson, Antarctica, and Adelaide, South Australia, J. Atm. Terr. Phys., 51, 761.
Plumb, R.A., 1983. Baroclinic instability of the summer mesosphere: A mechanism for the quasi-2-day wave?, J. Atmos. Sci., 40, 262.
Plumb, R.A., Hou, A.Y., 1992. The response of a zonally symmetric atmosphere to subtropical thermal forcing: Threshold behavior, J. Atmos. Sci., 49, 1790.
Poole, L. M. G., 1990. The characteristics of mesospheric two-day wave as observed at Grahamstown (33.3° S, 26.5° E), J. Atm. Terr. Phys., 52, 259.
Portnyagin, Y.I., Forbes, J.M., Merzlyakov, E.G., Makarov, N.A., Palo, S.E., 2000. Intra-diurnal wind variations observed in the lower thermosphere over the South Pole, Ann. Geophys., 18, 547.
Ruster, R., 1994. VHF radar observations of nonlinear interactions in the summer polar mesosphere, J. Atm. Terr. Phys., 561289.
Sivjee, G.G., Waltersheid, R.L., McEwen, D.J., 1994. Planetary wave disturbances in the Arctic winter mesospause over Eureka (80° N), Plan. Space Sci., 42, 973.
Smith, A.K., 1996. Longitudinal variations in mesospheric winds: Evidence for gravity wave filtering by planetary waves, J. Atmos. Sci., 53, 1156, 1996.
Smith, A.K., 1997. Stationary planetary waves in upper mesospheric winds, J. Atmos. Sci., 54, 2129.
Strobel, D.F., 1978. Parameterization of atmospheric heating rate from 15 to 120 km due to O2 and O3 absorption of solar radiation, J. Geophys. Res., 83, 7963.
Talaat, E.R., Lieberman, R., 1999. Non-migrating diurnal tides in mesospheric and lower thermospheric winds and temperatures J. Atmos. Sci., 56, 4073.

Talaat, E.R., Yee, J.H., Zhu, X., 2001. Observations of the 6.5-day wave in the mesosphere and lower thermosphere, J. Atmos. Sci., 106, 20715.
Talaat, E.R, and Mayr, H.G., 2010. Model of semi-diurnal pseudo-tide in the high-latitude upper mesosphere, Geophys. Res. Lett., in preparation.
Teitelbaum, H., Vial F., 1991. On tidal variability induced by nonlinear interaction with planetary waves, J. Geophys. Res., 96, 14,169-14,178.
Tsuda, T., Inoue, T., Fritts, D.C., VanZandt, T.E., Kato, S., Sato, T., Fukao, S., 1989. MST radar observations of a saturated gravity wave spectrum, J. Atm. Sci., 46, 2440.
Tsuda, T., Kato, S., Vincent, R.A., 1988. Long period oscillations observed by the Kyoto meteor radar and comparison of the quasi 2-day wave with Adelaide MF radar observations, J. Atm. Terr. Phys., 50, 225.
Vial, F., Forbes, J.M., 1989. Recent progress in tidal modeling, J. Atm. Terr. Phys., 51, 663.
Vincent, R.A., Kovalam, S., Fritts, D.C., Isler, J.R., 1998. Long-term MF radar observations of solar tide in the low-latitude mesosphere: Inter-annual variability and comparison with the GSWM, J. Geophys. Res., 103, 8667.
Volland, H., 1988. Atmospheric Tidal and Planetary Waves, Kluwer Academic Publ., Boston, MA.
Walterscheid, R.L., 1981. Inertio-gravity wave induced accelerations of mean flow having an imposed periodic component: Implications for tidal observations in the meteor region, J. Geophys. Res., 86, 9698-9706.
Wang, D.W., Ward, W.E., Shepherd, G.G., Wu, D.L., 2000. Stationary planetary waves inferred from WINDII wind data taken within altitudes 90-120 km during 1991-96, J. Atmos. Sci., 57, 1906.
Wehrbein, W.M., Leovy, C.B., 1982. An accurate radiative heating and cooling algorithm for use in a dynamical model of the middle atmosphere, J. Atmos. Sci., 39, 1532.
Wu, D.L., Jiang, J.H., 2005. Inter-annual and seasonal variations of diurnal tide, gravity waves, ozone, and water vapor as observed by MLS during 1991-1994, Adv. Space Res., 35, 1999.
Wu, D.L., et al., 1998. Equatorial diurnal variations observed in UARS microwave lib sounder temperature during 1991-1994 and simulated by the Canadian middle atmosphere model, J. Geophys. Res., 103, 8909.
Wu, Q., Killeen, T.T., McEwen, D., Solomon, S. C., Guo, W., Sivjee, G.G., Reeves, J.M., 2002. Observation of the mesospheric and lower thermospheric 10-h wave in the northern polar region, J. Geophys. Res., 107, 1082.
Wu, D. L., Hays, P.B. Skinner, W.R., et al., 1993. Observations of the quasi 2-day wave from the High Resolution Doppler Imager on UARS, Geophys. Res. Lett., 20, 2853.
Yudin, V.A., Khattatov, B.V., Geller, M. A., et al., 1997. Thermal tides and studies to tune the mechanistic tidal model using UARS observations, Ann. Geophys., 15, 1205.
Zhang, X., et al., 2006. Monthly tidal temperatures 20-120 km from TIMED/SABER, J. Geophys. Res., 111, A10S08, doi:10.1029/2005JA011504.
Zhu, X, 1989. Radiative cooling calculated by random band models with S-1-beta tailed distribution, J. Atmos. Sci., 46, 511.

Figure Captions:

Figure 1. Equatorial oscillations (QBO and SAO) generated with 2D (a) and 3D (b) versions of the NSM, applying identical GW sources. The QBO in the stratosphere (30 km), and the SAO in the mesosphere (55 and 80 km) have larger amplitudes in 2D. The GW amplify in 3D the tides and planetary waves at the expense of the QBO and SAO. (Figure taken from Mayr et al., 1999.)

Figure 2. Schematic diagram illustrates the processes that generate and influence the migrating and non-migrating tides, planetary-scale inertio gravity waves, and planetary waves. In the present paper, numerical experiments are discussed that illuminate the GW interactions enumerated.

Figure 3. Amplitude and phase of the diurnal tide generated with (a) and without (b) GW interactions. The GW increase the amplitudes and decrease the vertical wavelengths. (Figure taken from Mayr et al., 1998.)

Figure 4. Schematic diagram illustrating the GW interaction, which causes momentum deposition in regions of vertical wind shears, analogous to critical level absorption that produces the QBO. (Figure taken from Mayr et al., 1999.)

Figure 5. (a) Temporal variation of diurnal tide at 95 km and 18° latitude shows amplitude maxima near equinox. (b) The mean zonal winds change direction between 50 km and 80 km due to GW interaction, and their seasonal variations produce nodes close to equinox. During spring and fall, the GW propagate up without being much absorbed, and this produces semi-annual amplitude maxima in the diurnal tide (a). (Figure taken from Mayr et al., 1999.)

Figure 6. Amplitude and phase of the diurnal tide computed with and without GW interaction. (Figure taken from Mayr et al., 2001.)

Figure 7. (a) The planetary waves (PW) for m = 3 at 80 km peak around solstice, and they are amplified by GW. (b) Diurnal tide (DT) at 95 km computed with and without the m = 3 and 4 PW. The GW momentum expended on the PW is not available to amplify the DT, which produces lower amplitudes in summer. (Figures taken from Mayr et al., 2001.)

Figure 8. (a) Semidiurnal tide computed with and without GW. Like the diurnal tide (Fig. 6), the GW source causes amplification. (b) Semidiurnal tide computed with and without the excitation of the diurnal tide. During the spring and fall seasons, the GW amplify the diurnal tide at the expense of the semi-diurnal tide. (Figures taken from Mayr et al., 2001.)

Figure 9. Mean zonal winds in the lower stratosphere near the equator represent the QBO with a period of about 24 months (a). In the zonal winds of the diurnal tide at 95 km near the equator (b), the QBO periodicity is prevalent (c), and it appears also at 18° latitude where the tide peaks (d). (Figures taken from Mayr and Mengel, 2005.)

Figure 10. Normalized meridional (a) and vertical (b) advection terms generated by the QBO interacting with the diurnal tide. Pronounced QBO signatures are apparent but only at altitudes below about 60 km. (Figure taken from Mayr and Mengel, 2005.)

Figure 11. (a) Running average over 364 days for the mean zonal winds at 4° latitude. (b) Normalized GW momentum source, analogous to Fig. 10, shows inter-annual variations with a period close to 24

months extending into the upper mesosphere. (c) Amplitude of diurnal tide varies in phase with the GW momentum source. (Figure taken from Mayr and Mengel, 2005.)

Figure 12. Meridional winds at 100 km for the migrating and non-migrating diurnal tides. (a) The westward propagating tide peaks near 20° latitude, and the maxima near equinox exceed 90 m/s. (b) The eastward propagating tide for m = 1 is highly variable and peaks at the equator with amplitudes that approach 30 m/s. (c) The variable stationary tide for m = 0 is also confined to low latitudes, and its amplitudes can reach 40 m/s. (Figures taken from Mayr et al., 2005a.)

Figure 13. Non-migrating tides are produced in the NSM with planetary waves (PW) that are generated internally by instabilities in the zonal-mean. (a) The stationary diurnal tide for m = 0 is produced with m = 1 PW, and correlations are evident. (b) Without zonal-mean heat source, PW and non-migrating tide are not generated. (Figures taken from Mayr et al., 2003a.)

Figure 14. Illustration of proposed GW interaction for generating nonlinear coupling between migrating tides and PW. In the positive phase of the PW, for example, the eastward (positive) propagating GW are preferentially absorbed. The GW are then less effective in amplifying the eastward phase of the tide, which produces a non-migrating tide that is modulated by PW. (Figure taken from Mayr et al., 2005b.)

Figure 15. Non-migrating m = 0 tide generated with and without GW interaction. (Figure taken from Mayr et al., 2005b.)

Figure 16. Computer experiment with standard and time independent m = 0 GW source. (a) The migrating tide (m = 1) is not affected. (b) With constant GW source (lower panel), the PW amplitudes are larger. (c) Non-migrating tide generated with migrating tide (a) and PW (b). The time dependence of the GW source produces a much larger tide, although the PW involved are somewhat weaker. This demonstrates the importance of GW for the non-linear coupling between migrating tide and PW. (Figures taken from Mayr et al., 2005b.)

Figure 17. Oscillations for m = 1 at high latitudes are shown with periods around 10 hours. Like tides, the waves grow with height and have vertical wavelengths of about 20 km. The amplitudes of meridional winds (a, b) and temperature variations approach in the upper mesosphere 40 m/s and 5 K, respectively. (Figures taken from Mayr et al., 2003b, 2004b.)

Figure 18. Meridional wind spectrum for m = 1at 100 km shows westward propagating 12-hour semi-diurnal tide. Oscillations around 9 and 10 hours propagating westward at polar latitudes, and 9-hour waves propagating eastward at mid latitudes. (Figure taken from Mayr et al., 2004b.)

Figure 19. (a) Seasonal variations of westward and eastward propagating 10-hour waves show peak amplitudes during winter and spring seasons. (b) Without excitation of diurnal tides, 10-hour waves are generated with comparable amplitudes, but the seasonal variations are different. (Figures taken from Mayr et al., 2004b.)

Figure 20. (a) Temperature variations for December solstice show a pattern in qualitative agreement with observations. (b) Reversing latitudinal temperature variations, and related meridional circulation, are conducive for generating baroclinic instabilities in the troposphere and middle atmosphere, which produces the planetary waves in the model. (Figure taken from Mayr et al., 2004a.)

Figure 21. Planetary waves at 90 km and mid latitudes for m = 1 and 3, generated with tropospheric source (a) and without (b). (Figures taken from Mayr et al., 2004a.)

Figure 22. Planetary waves for m = 3 at 60 and 90 km show changing patterns of seasonal variations. Peaks occur in winter at 60 km, and in summer at 90 km. (Figures taken from Mayr et al., 2004a.)

Figure 23. Meridional gradients of m = 0 pressure and density are measures of baroclinic instability. Peaks occur in winter at 50 km (a) but in summer at 90 km (b), which is consistent with the changing planetary wave patterns in Fig. 22. (Figures taken from Mayr et al., 2004a.)

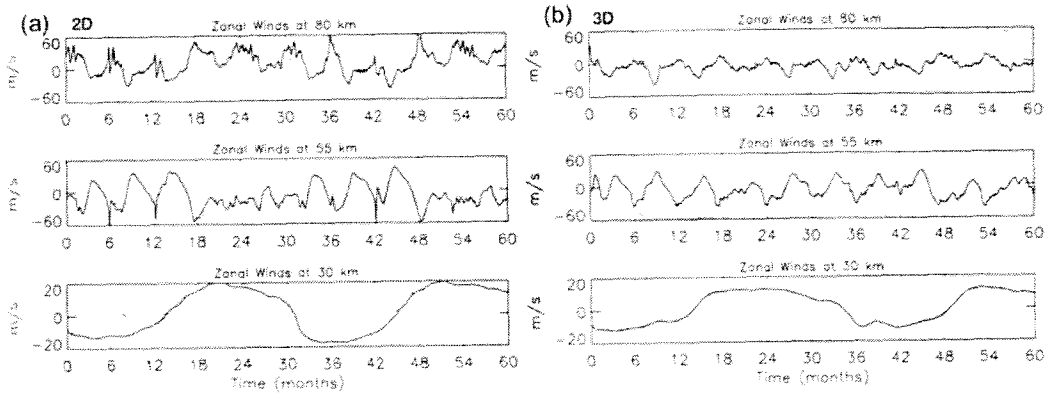
(a) 2D
Zonal Winds at 80 km
Zonal Winds at 55 km
Zonal Winds at 30 km
m/s
Time (months)
(b) 3D
Zonal Winds at 80 km
Zonal Winds at 55 km
Zonal Winds at 30 km
m/s
Time (months)

Figure 1

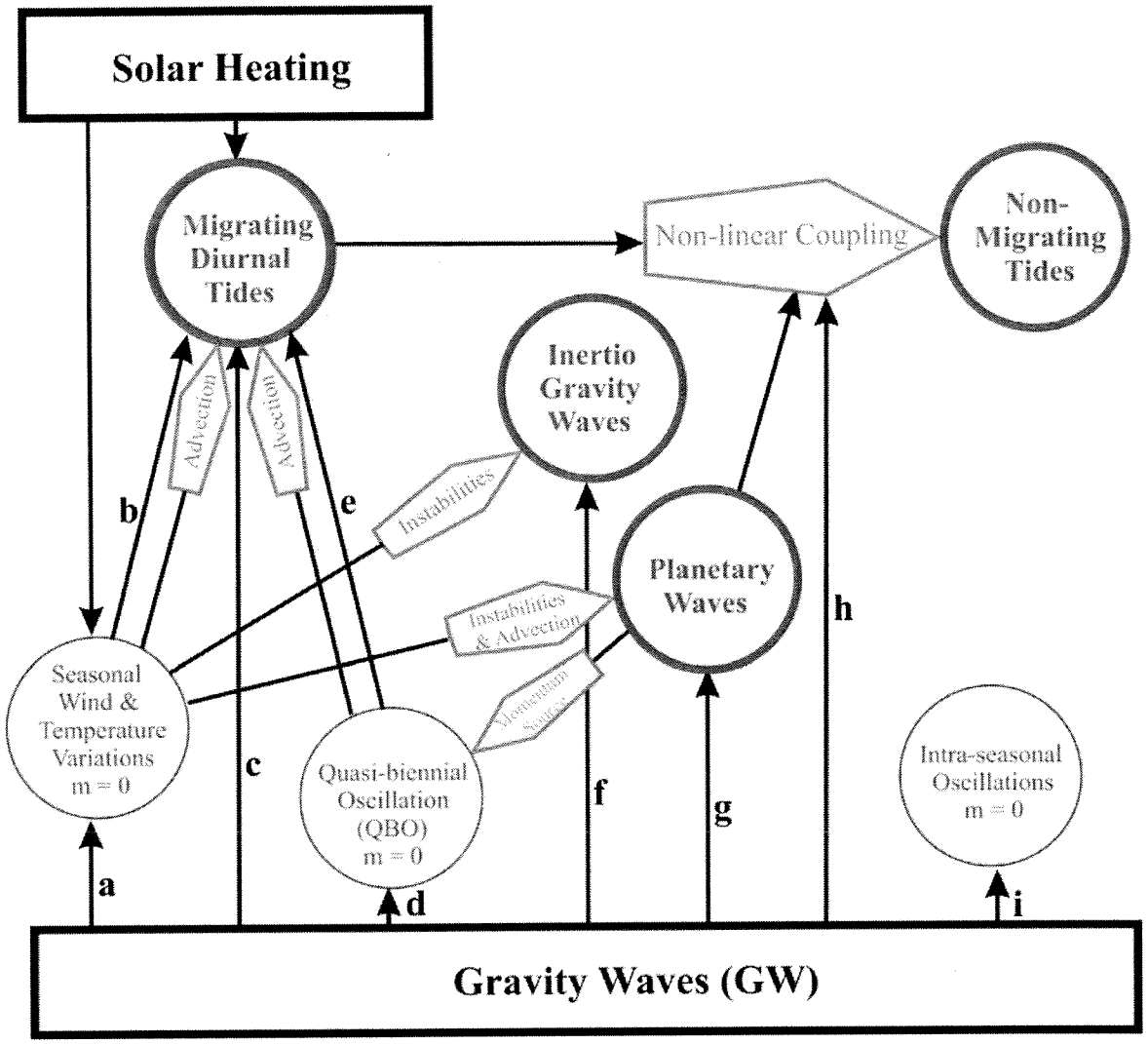

(a) GW interaction produces temperature and wind reversals that lead to instabilities
(b) GW filtering produces seasonal variations
(c) GW interaction amplifies tides
(d) GW source of QBO
(e) GW filtering produces inter-annual variations
(f) GW source amplifies planetary-scale inertio gravity waves
(g) GW interaction amplifies planetary waves
(h) GW filtering contributes to nonlinear interaction between migrating tides and planetary waves
(i) GW source of intra-seasonal (2-month) oscillations

Figure 2

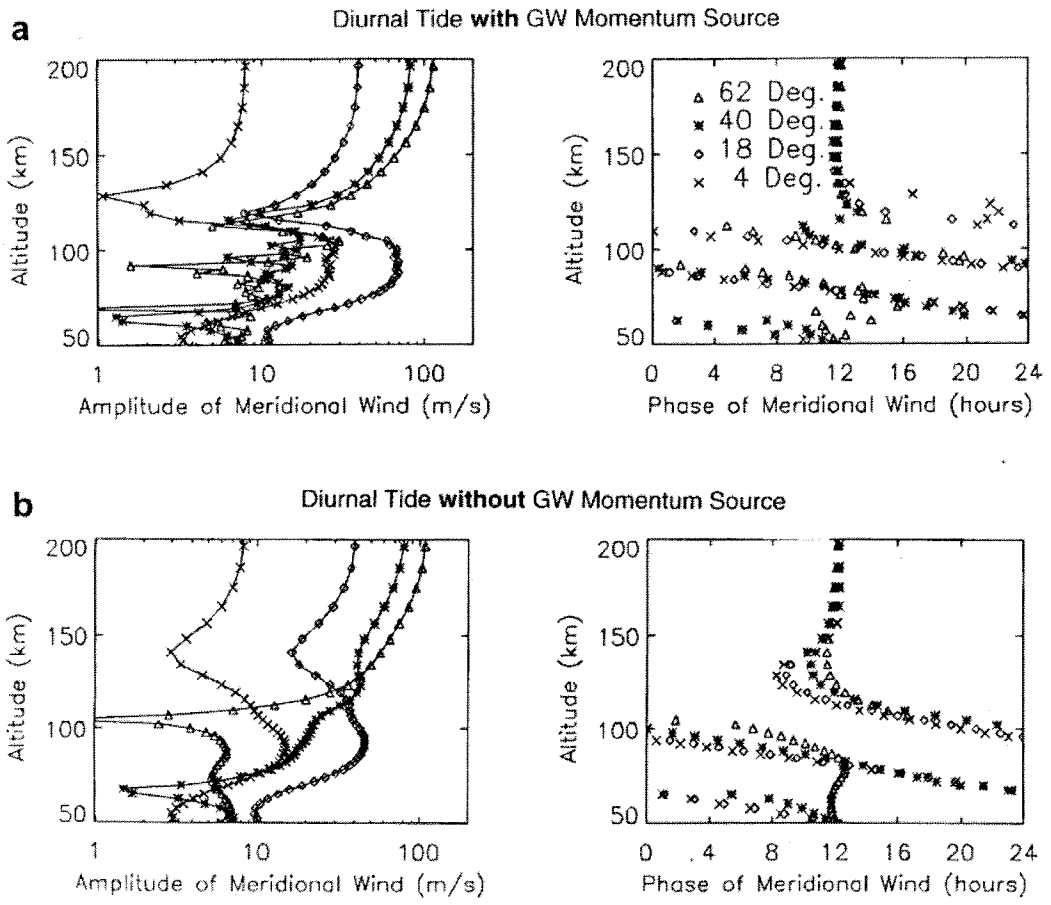
a
Diurnal Tide with GW Momentum Source
Altitude (km)
200
150
100
50
1
10
100
Amplitude of Meridional Wind (m/s)
62 Deg.
40 Deg.
18 Deg.
4 Deg.
0
4
8
12
16
20
24
Phase of Meridional Wind (hours)
b
Diurnal Tide without GW Momentum Source

Figure 3

Gravity Wave Interaction with Tide

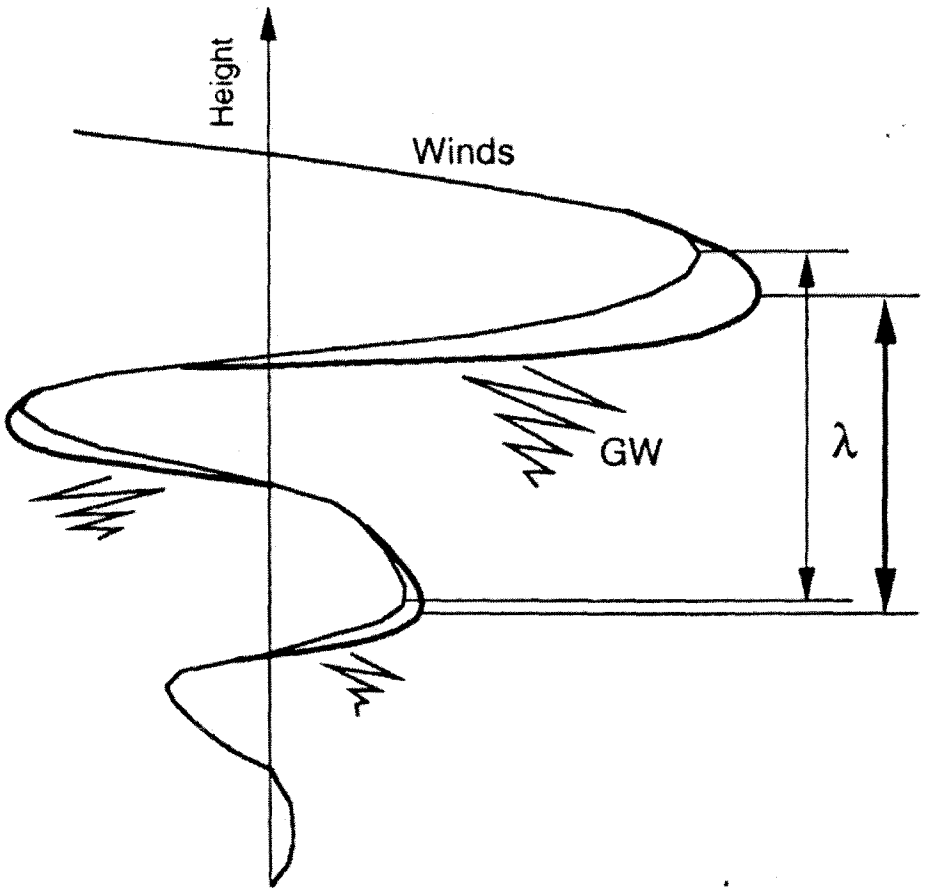

Figure 4

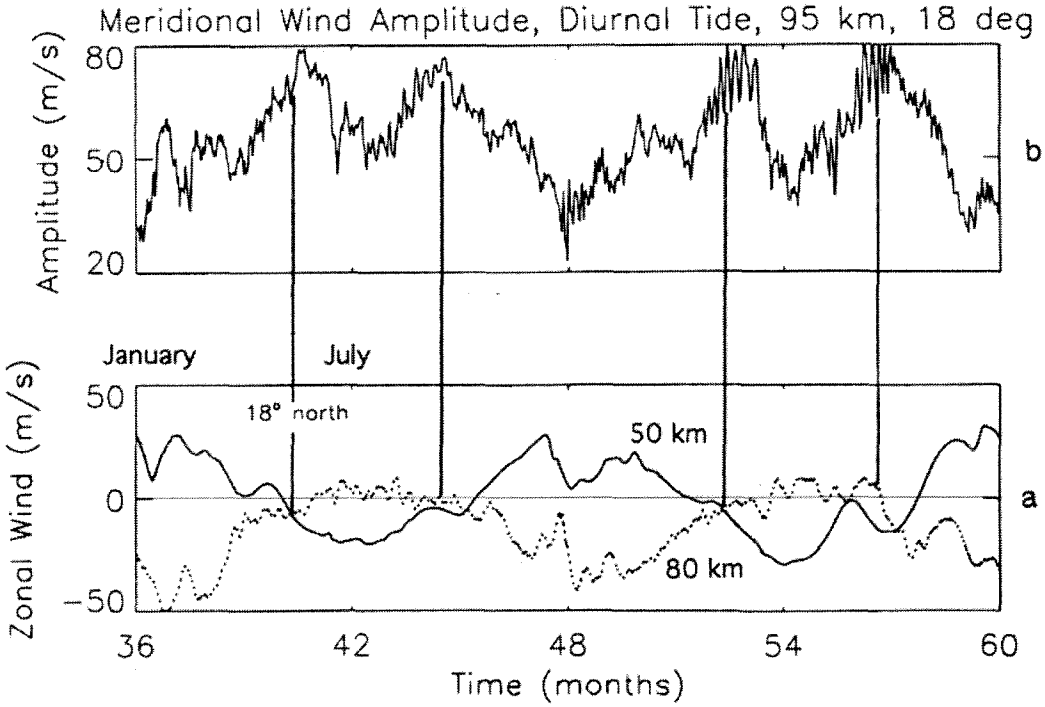
Meridional Wind Amplitude, Diurnal Tide, 95 km, 18 deg
Amplitude (m/s)
80
50
20
b
January
July
Zonal Wind (m/s)
50
18° north
50 km
0
a
80 km
−50
36
42
48
54
60
Time (months)

Figure 5

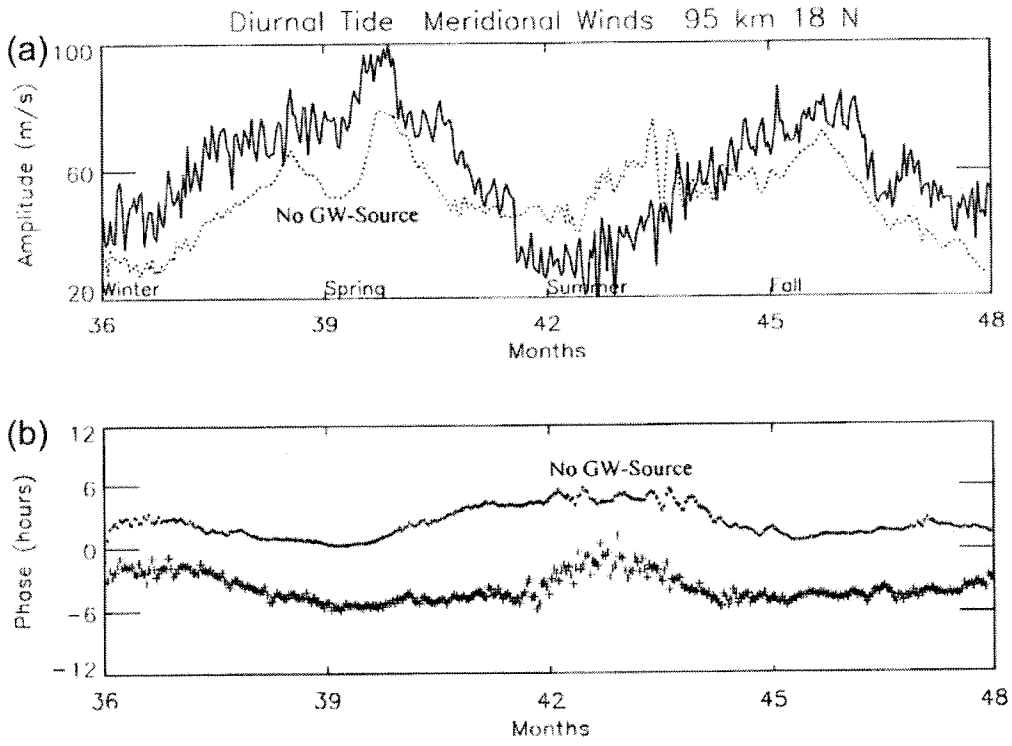
Diurnal Tide Meridional Winds 95 km 18 N
(a)
Amplitude (m/s)
100
60
20
No GW-Source
Winter
Spring
Summer
Fall
36
39
42
45
48
Months
(b)
Phase (hours)
12
6
0
-6
-12
No GW-Source
36
39
42
45
48
Months

Figure 6

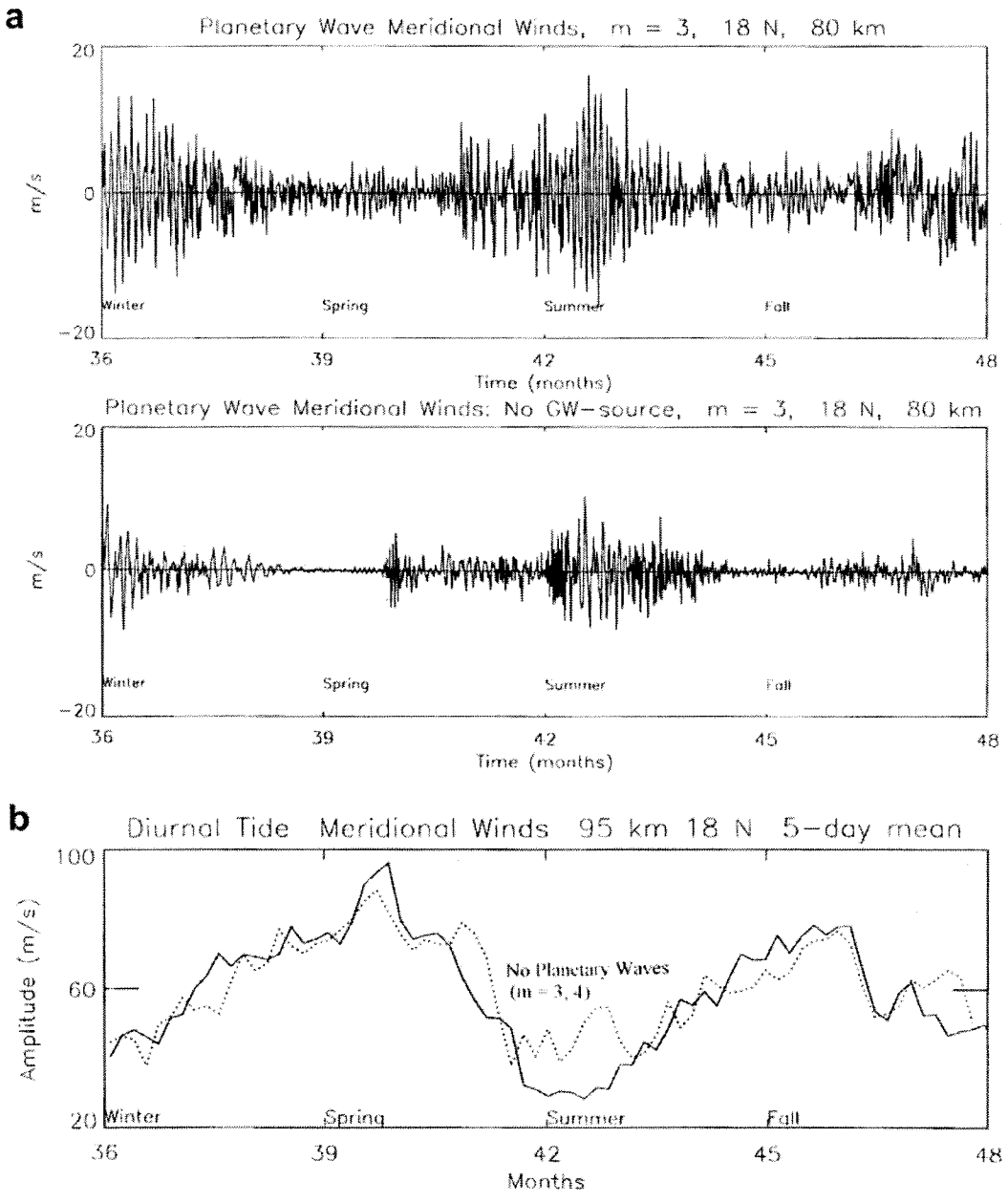
a
Planetary Wave Meridional Winds, m = 3, 18 N, 80 km
20
0
-20
m/s
Winter
Spring
Summer
Fall
36
39
42
45
48
Time (months)
Planetary Wave Meridional Winds: No GW-source, m = 3, 18 N, 80 km
20
0
-20
m/s
Winter
Spring
Summer
Fall
36
39
42
45
48
Time (months)
b
Diurnal Tide Meridional Winds 95 km 18 N 5-day mean
100
60
20
Amplitude (m/s)
No Planetary Waves
(m = 3, 4)
Winter
Spring
Summer
Fall
36
39
42
45
48
Months

Figure 7

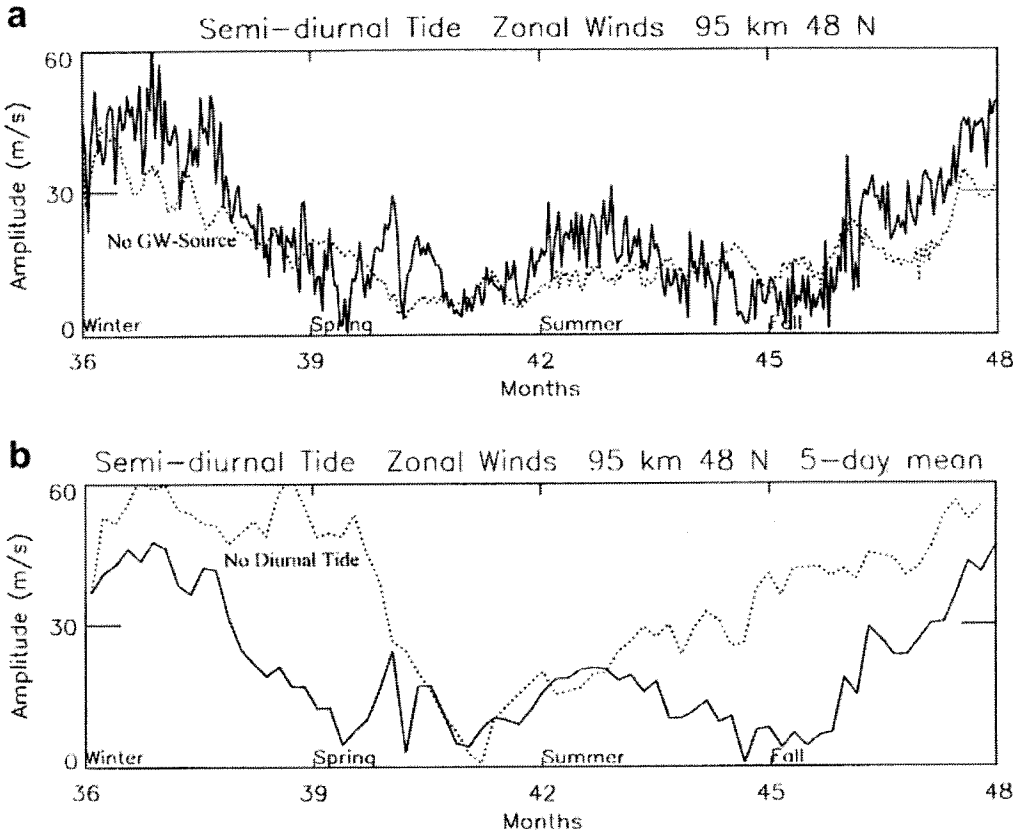
a
Semi-diurnal Tide Zonal Winds 95 km 48 N
Amplitude (m/s)
60
30
0
No GW-Source
Winter
Spring
Summer
Fall
36
39
42
45
48
Months
b
Semi-diurnal Tide Zonal Winds 95 km 48 N 5-day mean
Amplitude (m/s)
60
30
0
No Diurnal Tide
Winter
Spring
Summer
Fall
36
39
42
45
48
Months

Figure 8

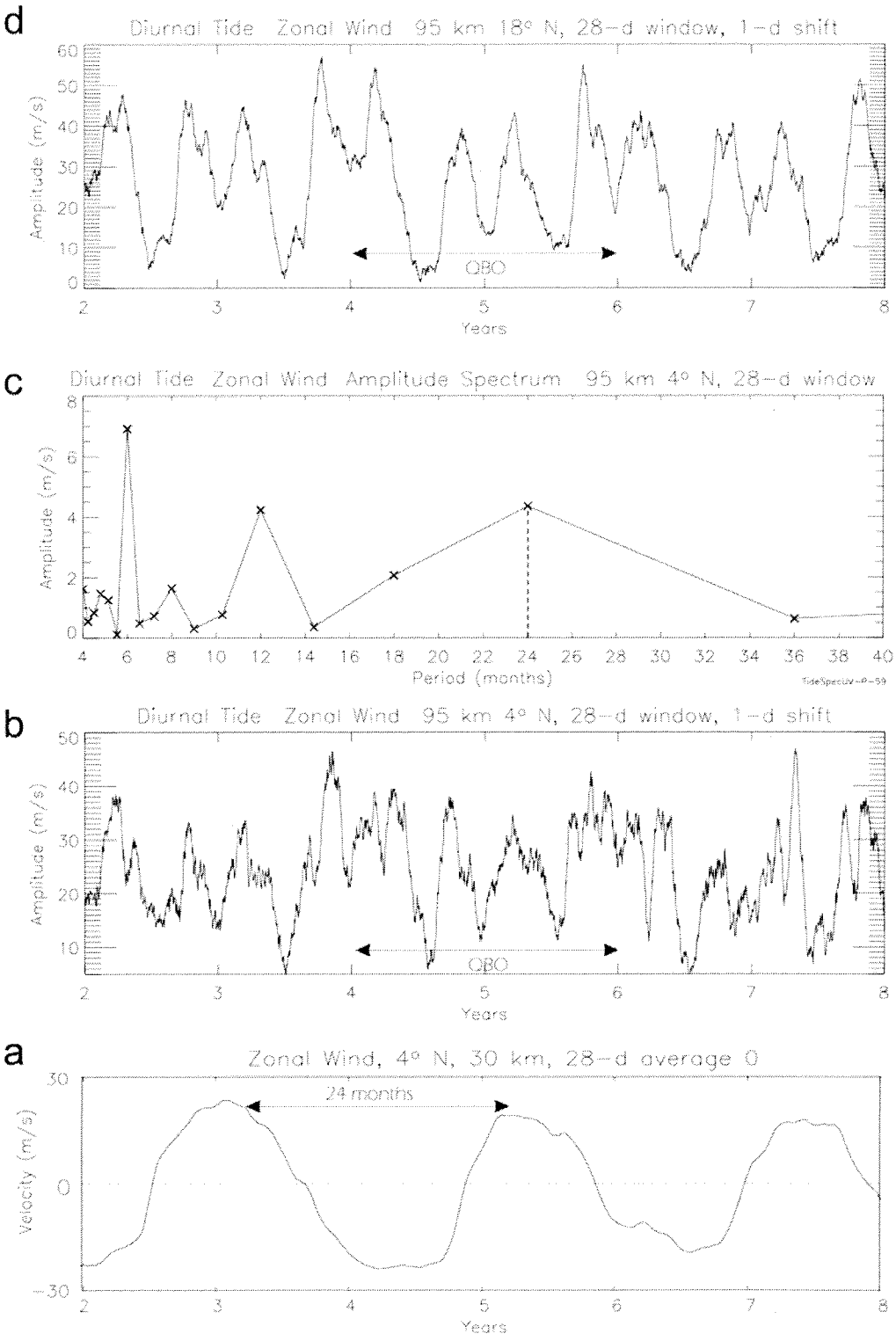
d
Diurnal Tide Zonal Wind 95 km 18° N, 28-d window, 1-d shift
Amplitude (m/s)
QBO
Years
c
Diurnal Tide Zonal Wind Amplitude Spectrum 95 km 4° N, 28-d window
Amplitude (m/s)
Period (months)
b
Diurnal Tide Zonal Wind 95 km 4° N, 28-d window, 1-d shift
Amplitude (m/s)
QBO
Years
a
Zonal Wind, 4° N, 30 km, 28-d average 0
24 months
Velocity (m/s)
Years

Figure 9

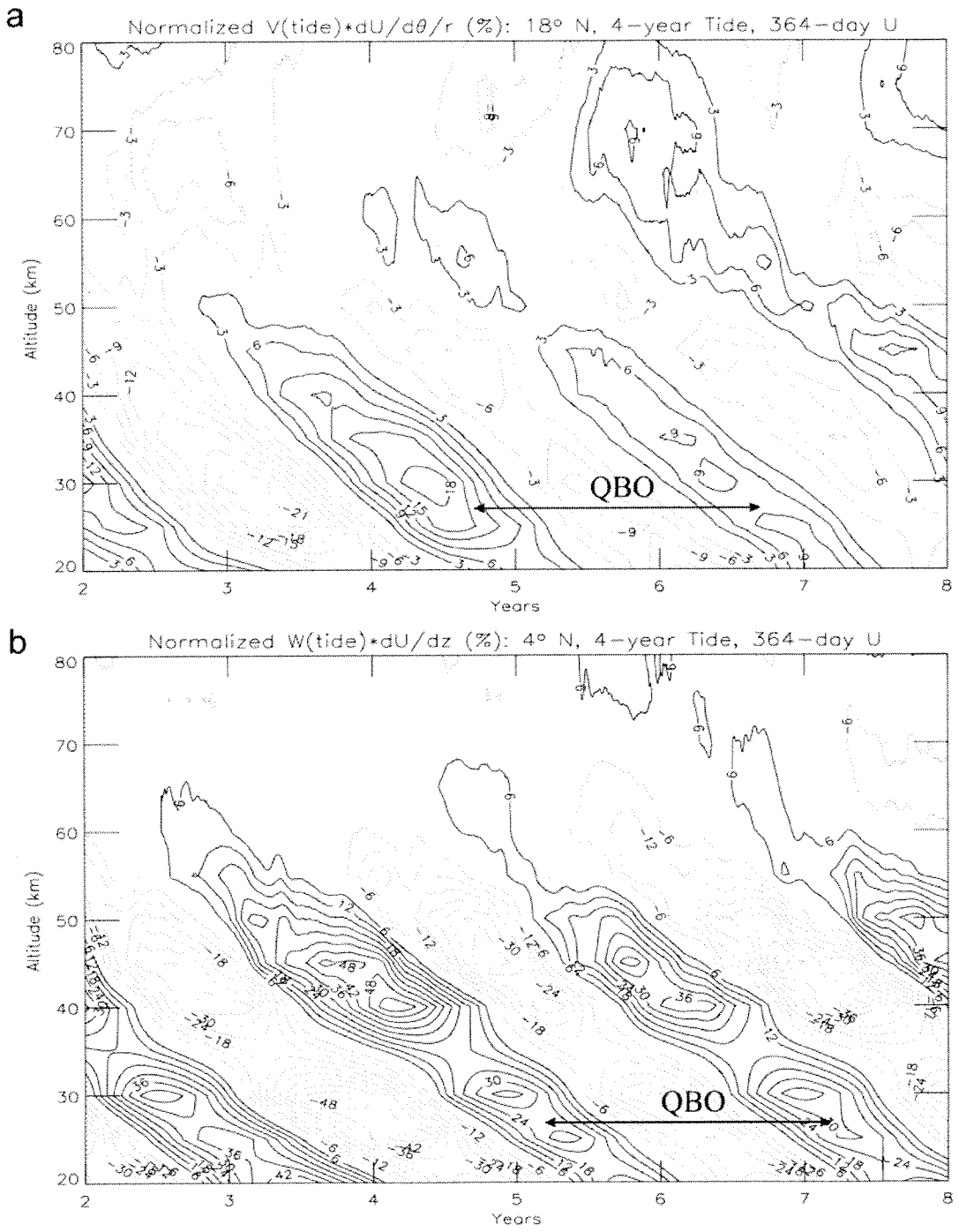
a
Normalized V(tide)*dU/dθ/r (%): 18° N, 4-year Tide, 364-day U
Altitude (km)
Years
QBO
b
Normalized W(tide)*dU/dz (%): 4° N, 4-year Tide, 364-day U
Altitude (km)
Years
QBO

Figure 10

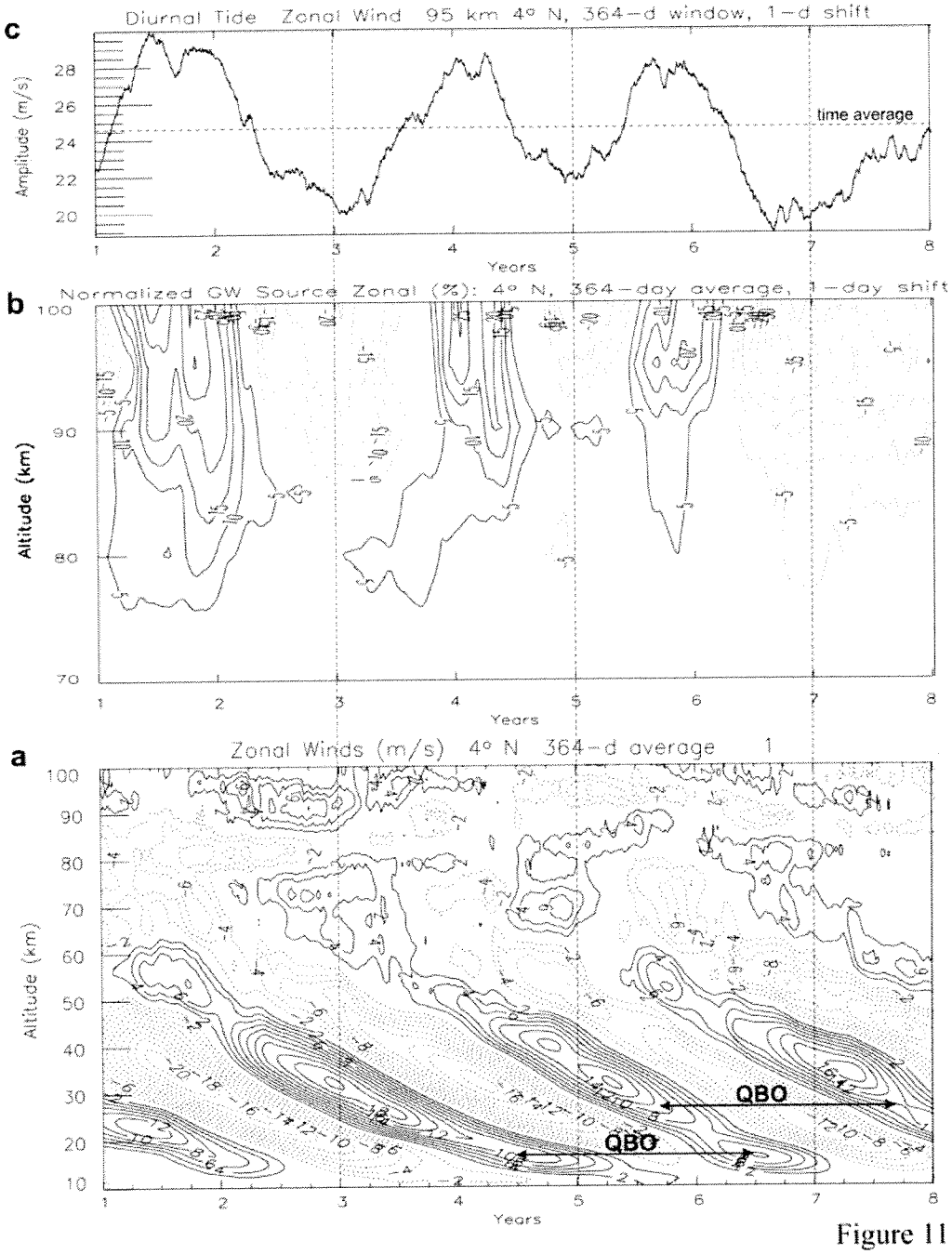
c
Diurnal Tide Zonal Wind 95 km 4° N, 364-d window, 1-d shift
Amplitude (m/s)
time average
Years
b
Normalized GW Source Zonal (%): 4° N, 364-day average, 1-day shift
Altitude (km)
Years
a
Zonal Winds (m/s) 4° N 364-d average 1
Altitude (km)
QBO
QBO
Years

Figure 11

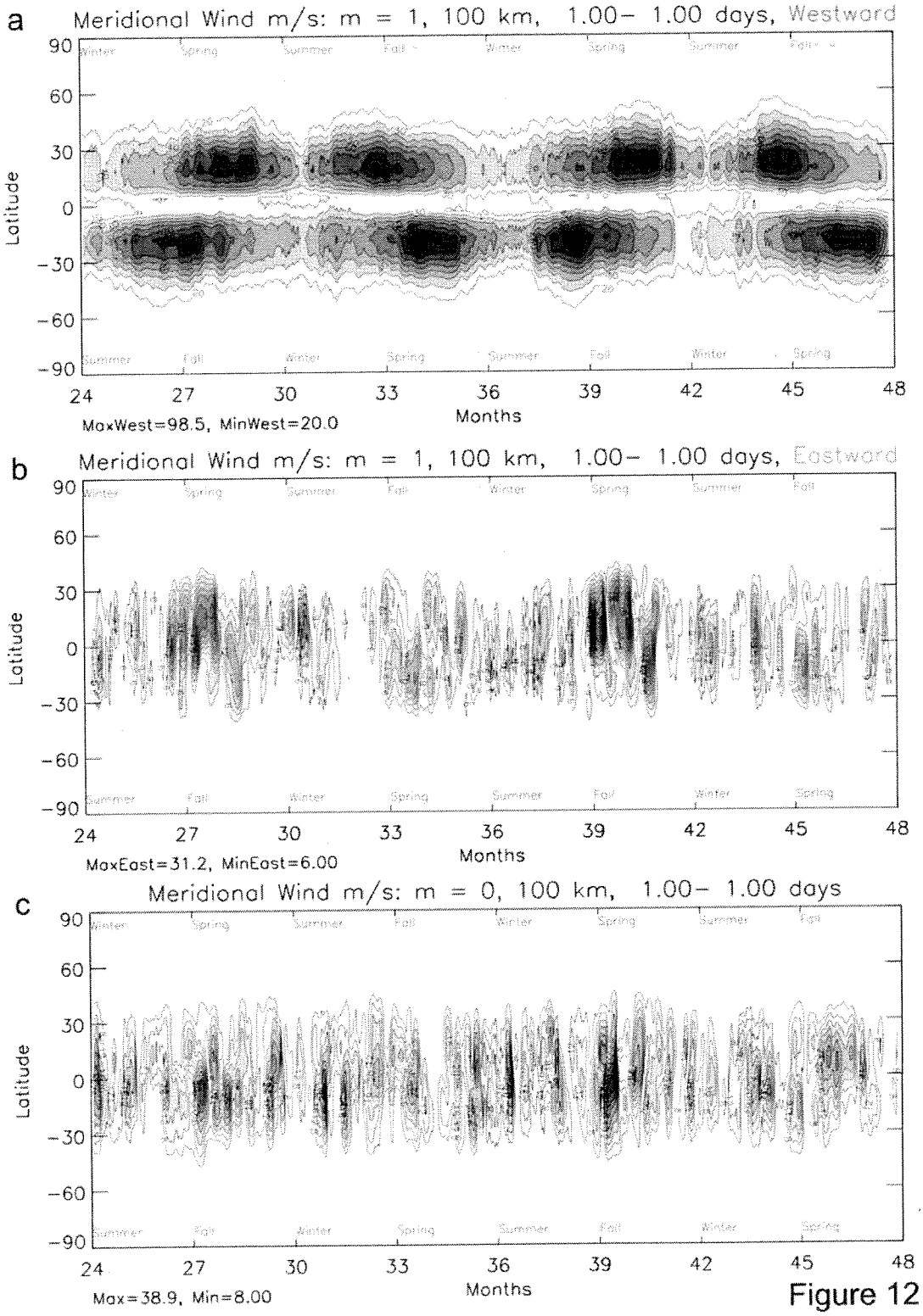
a
Meridional Wind m/s: m = 1, 100 km, 1.00– 1.00 days, Westward
Latitude
Months
MaxWest=98.5, MinWest=20.0
b
Meridional Wind m/s: m = 1, 100 km, 1.00– 1.00 days, Eastward
Latitude
Months
MaxEast=31.2, MinEast=6.00
c
Meridional Wind m/s: m = 0, 100 km, 1.00– 1.00 days
Latitude
Months
Max=38.9, Min=8.00

Figure 12

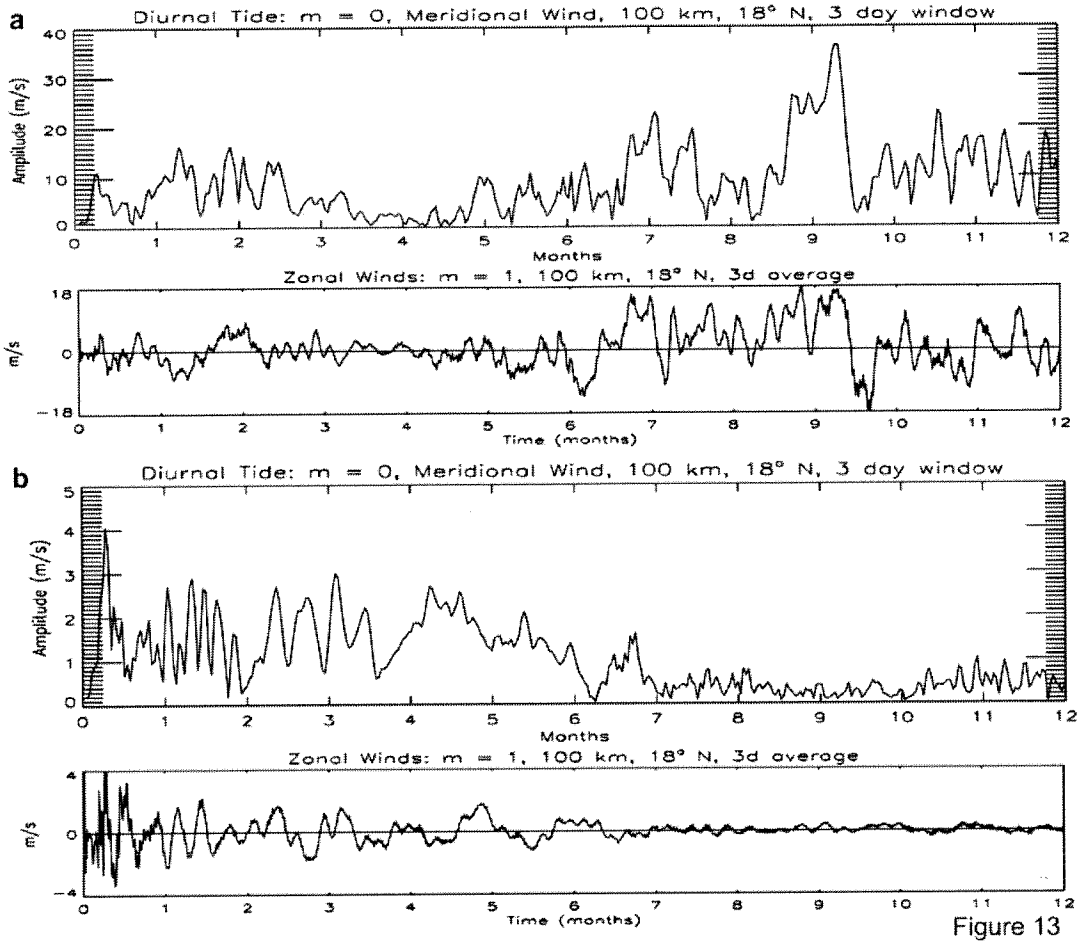
a
Diurnal Tide: m = 0, Meridional Wind, 100 km, 18° N, 3 day window
Amplitude (m/s)
Months
Zonal Winds: m = 1, 100 km, 18° N, 3d average
m/s
Time (months)
b
Diurnal Tide: m = 0, Meridional Wind, 100 km, 18° N, 3 day window
Amplitude (m/s)
Months
Zonal Winds: m = 1, 100 km, 18° N, 3d average
m/s
Time (months)

Figure 13

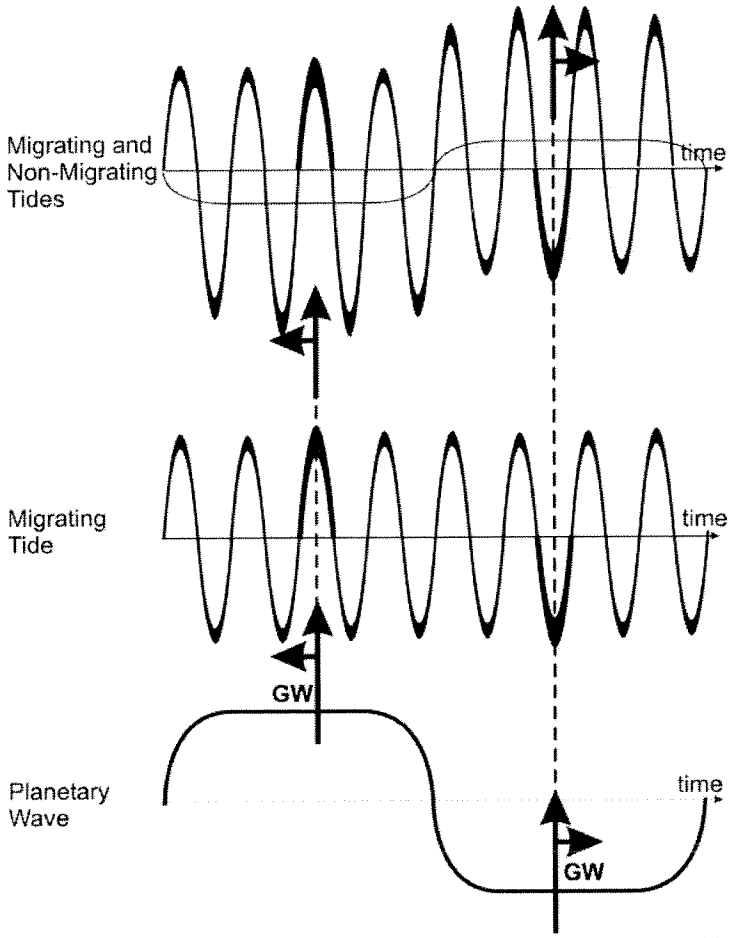
Migrating and
Non-Migrating
Tides
time
Migrating
Tide
time
GW
Planetary
Wave
time
GW

Figure 14

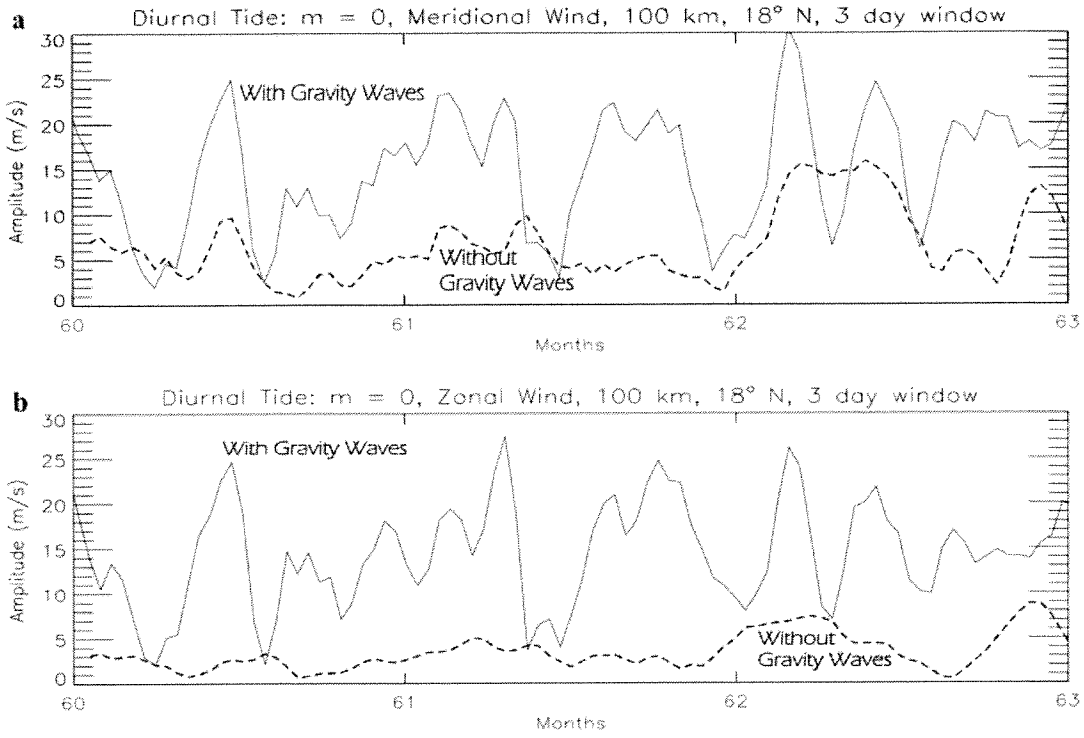
a
Diurnal Tide: m = 0, Meridional Wind, 100 km, 18° N, 3 day window
Amplitude (m/s)
With Gravity Waves
Without
Gravity Waves
Months
b
Diurnal Tide: m = 0, Zonal Wind, 100 km, 18° N, 3 day window
Amplitude (m/s)
With Gravity Waves
Without
Gravity Waves
Months

Figure 15

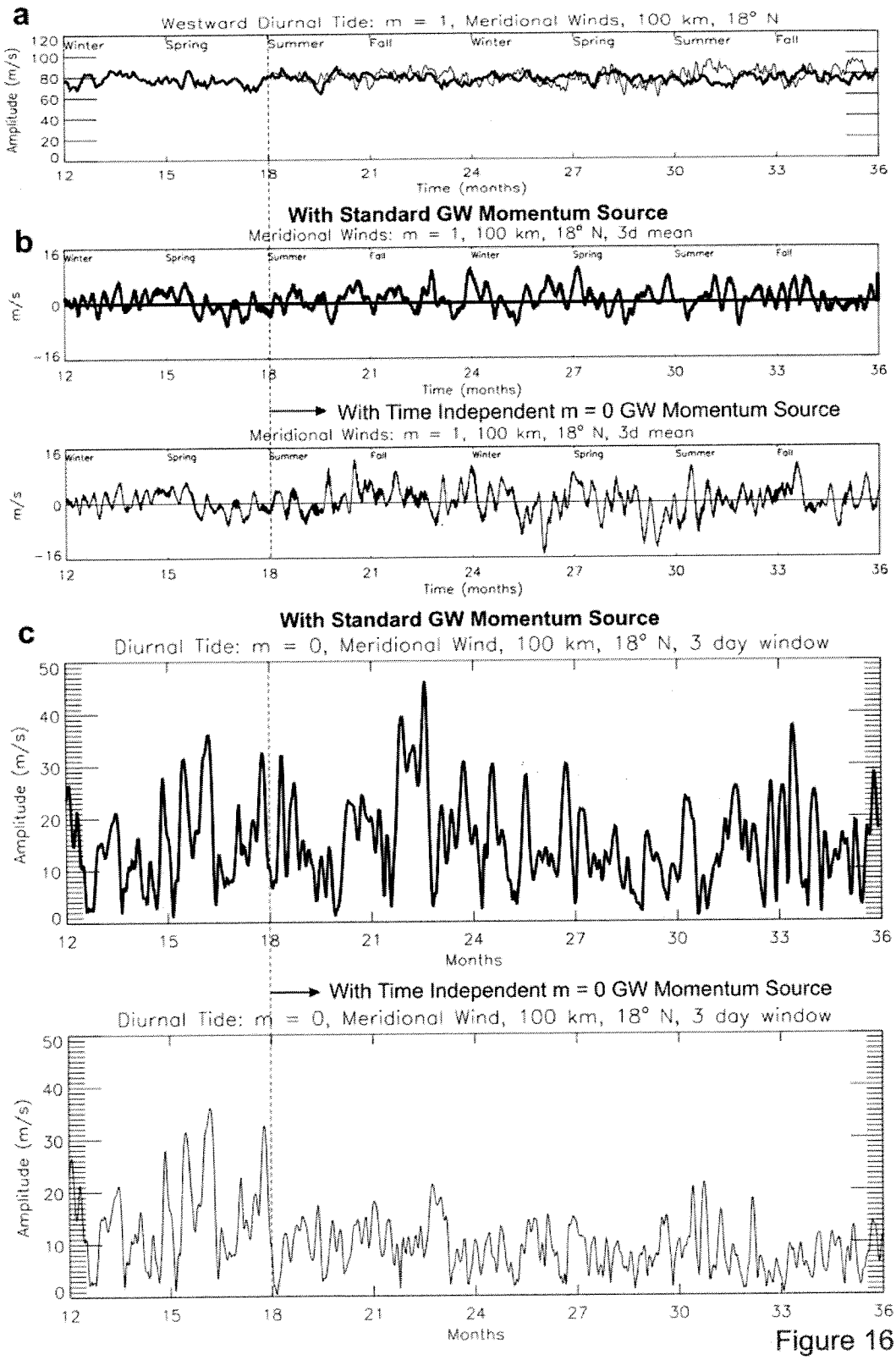
a
Westward Diurnal Tide: m = 1, Meridional Winds, 100 km, 18° N
Winter
Spring
Summer
Fall
Winter
Spring
Summer
Fall
Amplitude (m/s)
Time (months)
With Standard GW Momentum Source
b
Meridional Winds: m = 1, 100 km, 18° N, 3d mean
m/s
Time (months)
With Time Independent m = 0 GW Momentum Source
Meridional Winds: m = 1, 100 km, 18° N, 3d mean
m/s
Time (months)
With Standard GW Momentum Source
c
Diurnal Tide: m = 0, Meridional Wind, 100 km, 18° N, 3 day window
Amplitude (m/s)
Months
With Time Independent m = 0 GW Momentum Source
Diurnal Tide: m = 0, Meridional Wind, 100 km, 18° N, 3 day window
Amplitude (m/s)
Months

Figure 16

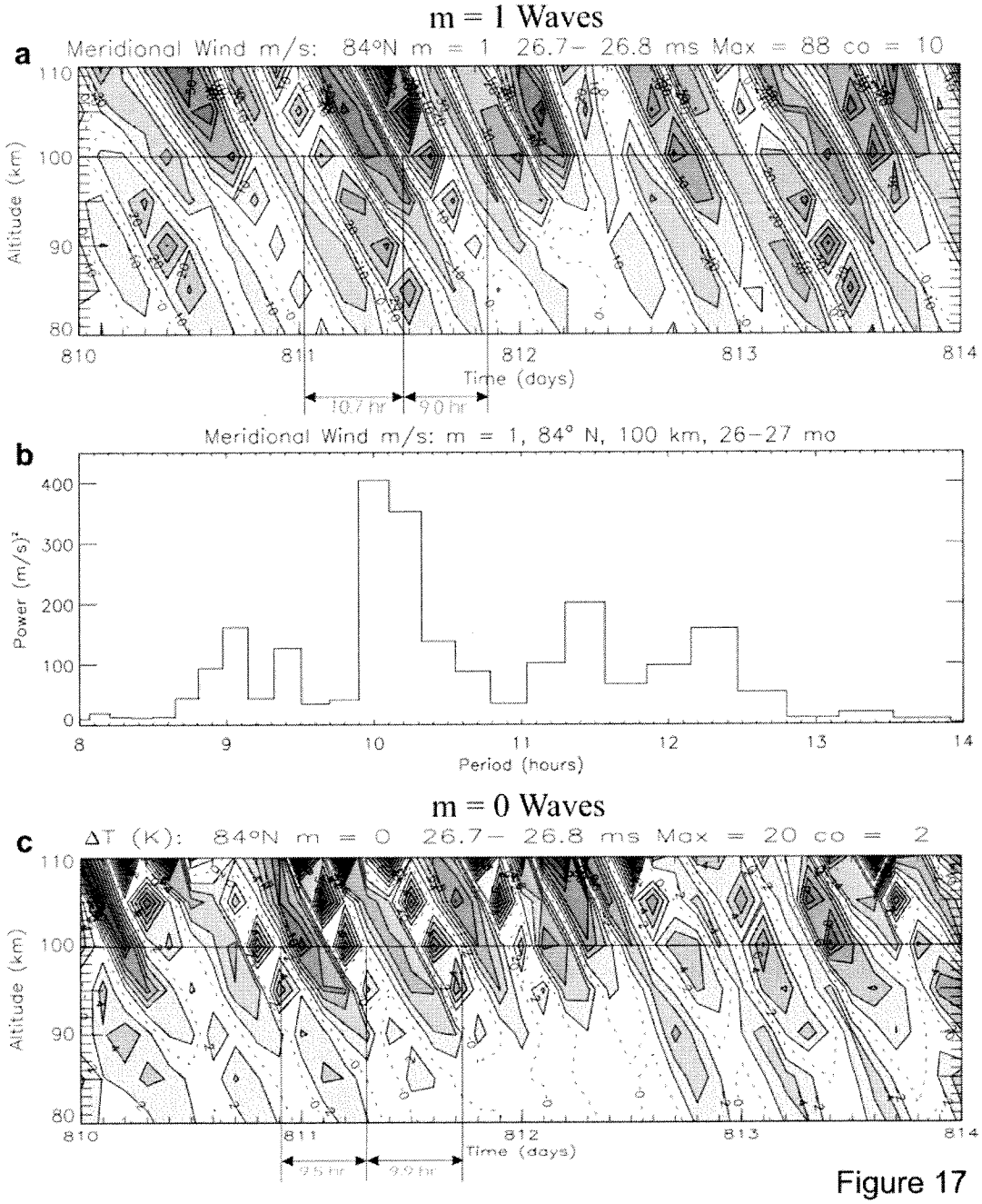
m = 1 Waves
a
Meridional Wind m/s: 84°N m = 1 26.7– 26.8 ms Max = 88 co = 10
Altitude (km)
110
100
90
80
810
811
812
813
814
Time (days)
10.7 hr
9.0 hr
Meridional Wind m/s: m = 1, 84° N, 100 km, 26–27 mo
b
Power (m/s)²
400
300
200
100
0
8
9
10
11
12
13
14
Period (hours)
m = 0 Waves
c
ΔT (K): 84°N m = 0 26.7– 26.8 ms Max = 20 co = 2
Altitude (km)
110
100
90
80
810
811
812
813
814
Time (days)
9.5 hr
9.0 hr

Figure 17

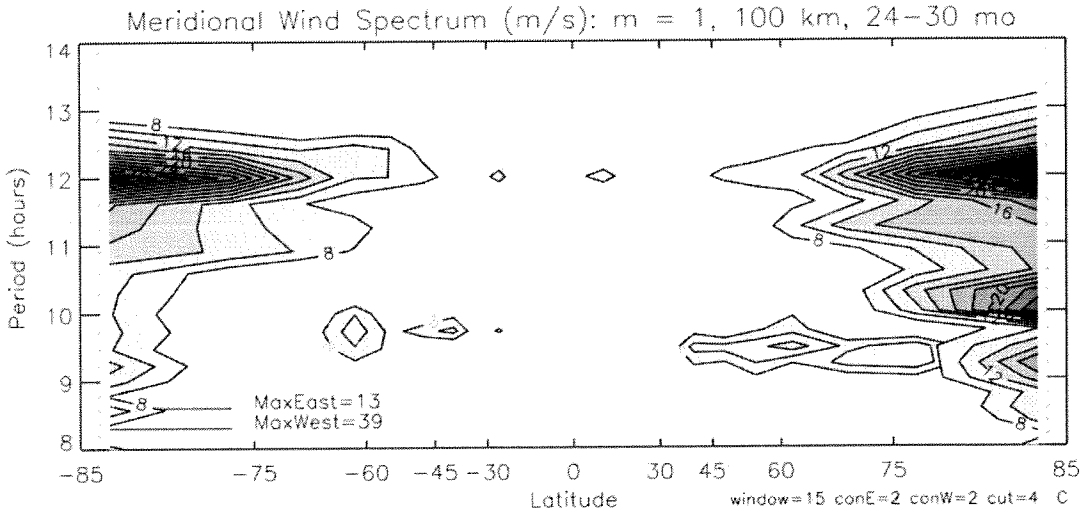
Meridional Wind Spectrum (m/s): m = 1, 100 km, 24-30 mo
Period (hours)
14
13
12
11
10
9
8
MaxEast=13
MaxWest=39
-85
-75
-60
-45
-30
0
30
45
60
75
85
Latitude
window=15 conE=2 conW=2 cut=4

Figure 18

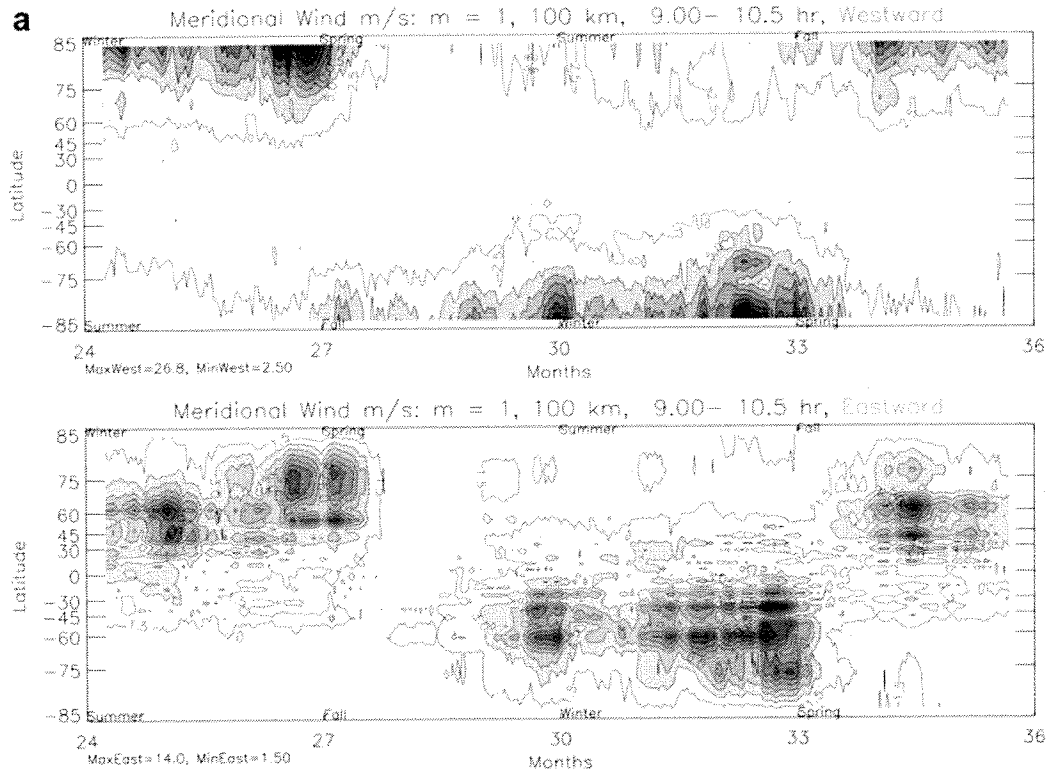

Without Excitation of Migrating Diurnal Tides

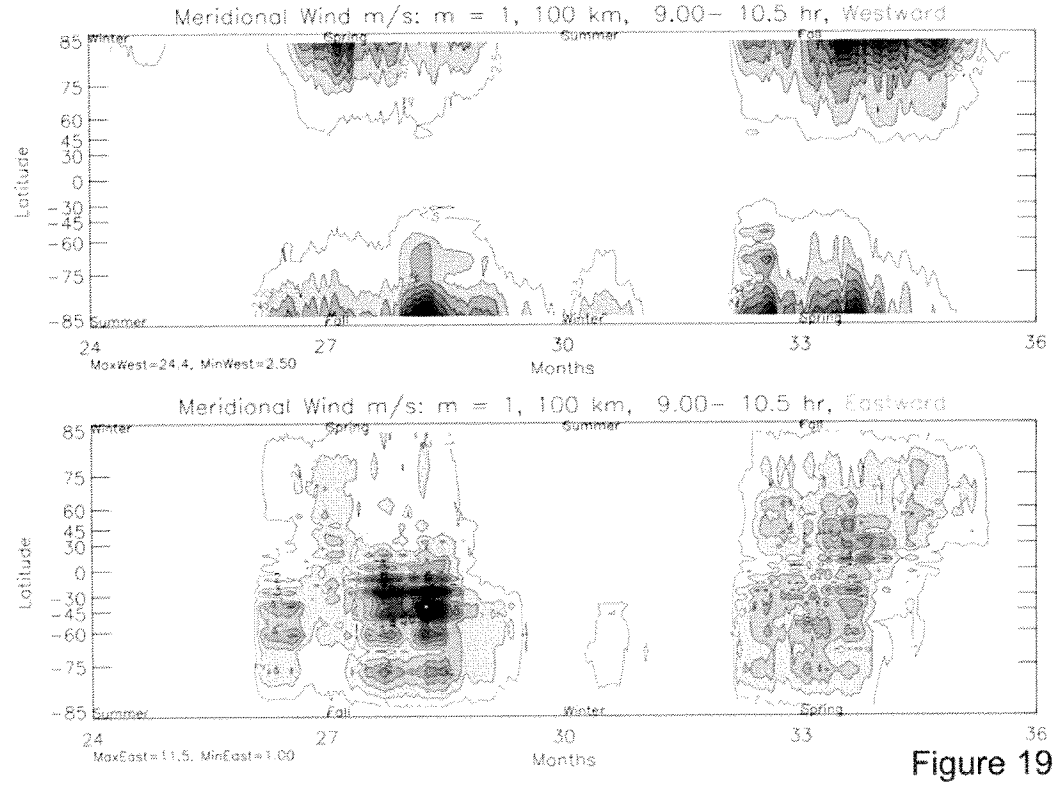

Figure 19

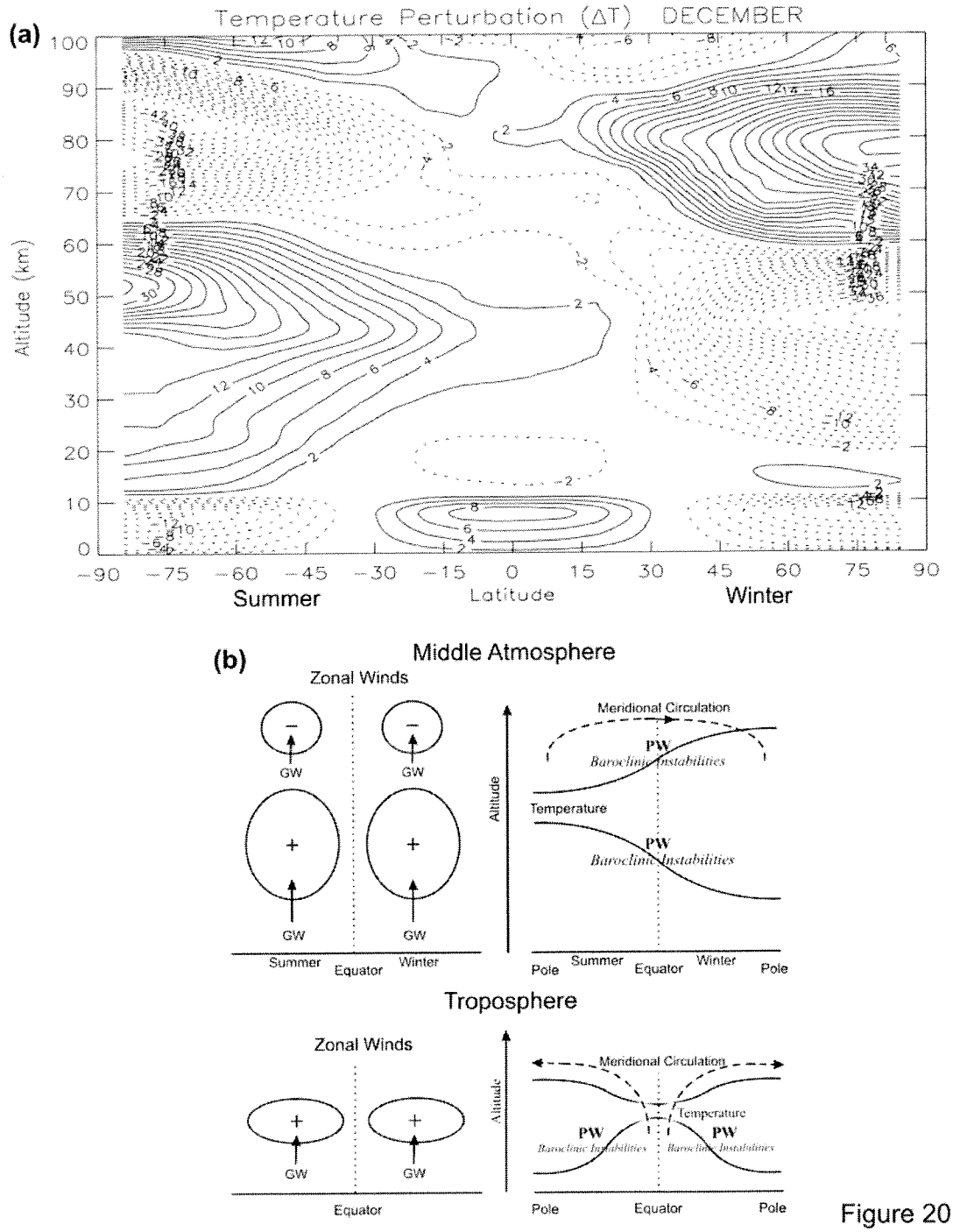
(a)
Temperature Perturbation (ΔT) DECEMBER
Altitude (km)
100
90
80
70
60
50
40
30
20
10
0
−90 −75 −60 −45 −30 −15 0 15 30 45 60 75 90
Summer
Latitude
Winter
(b)
Middle Atmosphere
Zonal Winds
GW
GW
GW
GW
Summer
Equator
Winter
Altitude
Meridional Circulation
PW
Baroclinic Instabilities
Temperature
PW
Baroclinic Instabilities
Pole
Summer
Equator
Winter
Pole
Troposphere
Zonal Winds
GW
GW
Equator
Altitude
Meridional Circulation
Temperature
PW
Baroclinic Instabilities
PW
Baroclinic Instabilities
Pole
Equator
Pole

Figure 20

a With Troposphere & Middle Atmosphere Zonal Mean (m = 0) Heat Source

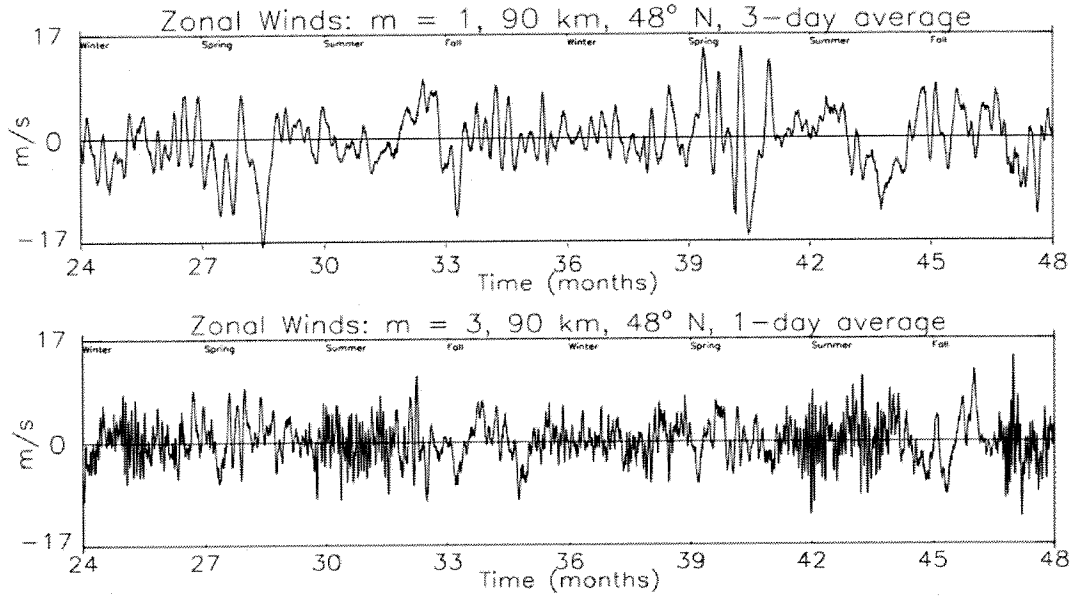

b Without Troposphere Zonal Mean (m = 0) Heat Source

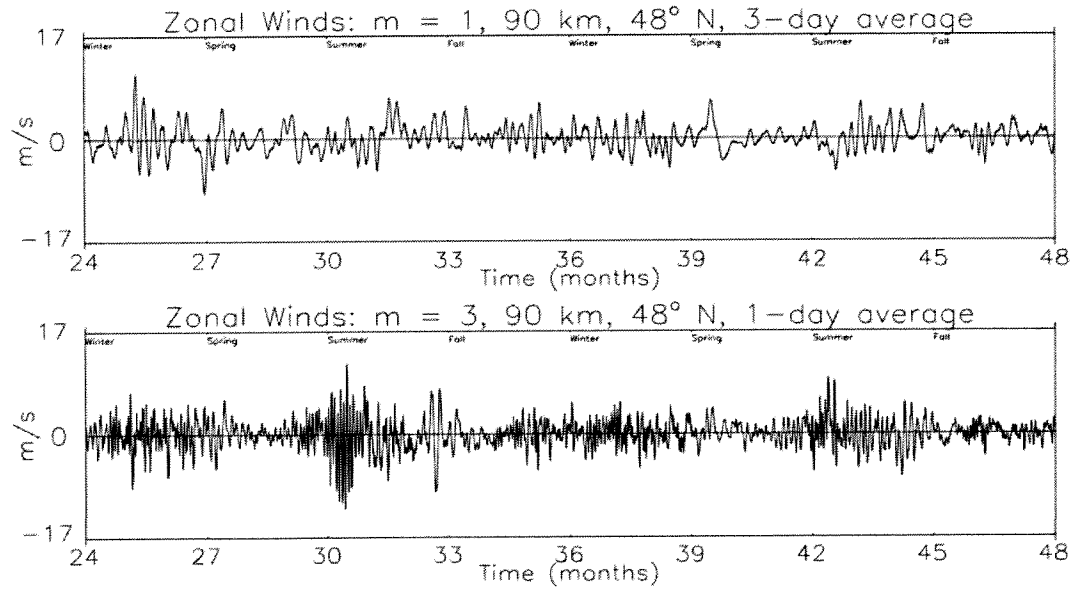

Figure 21

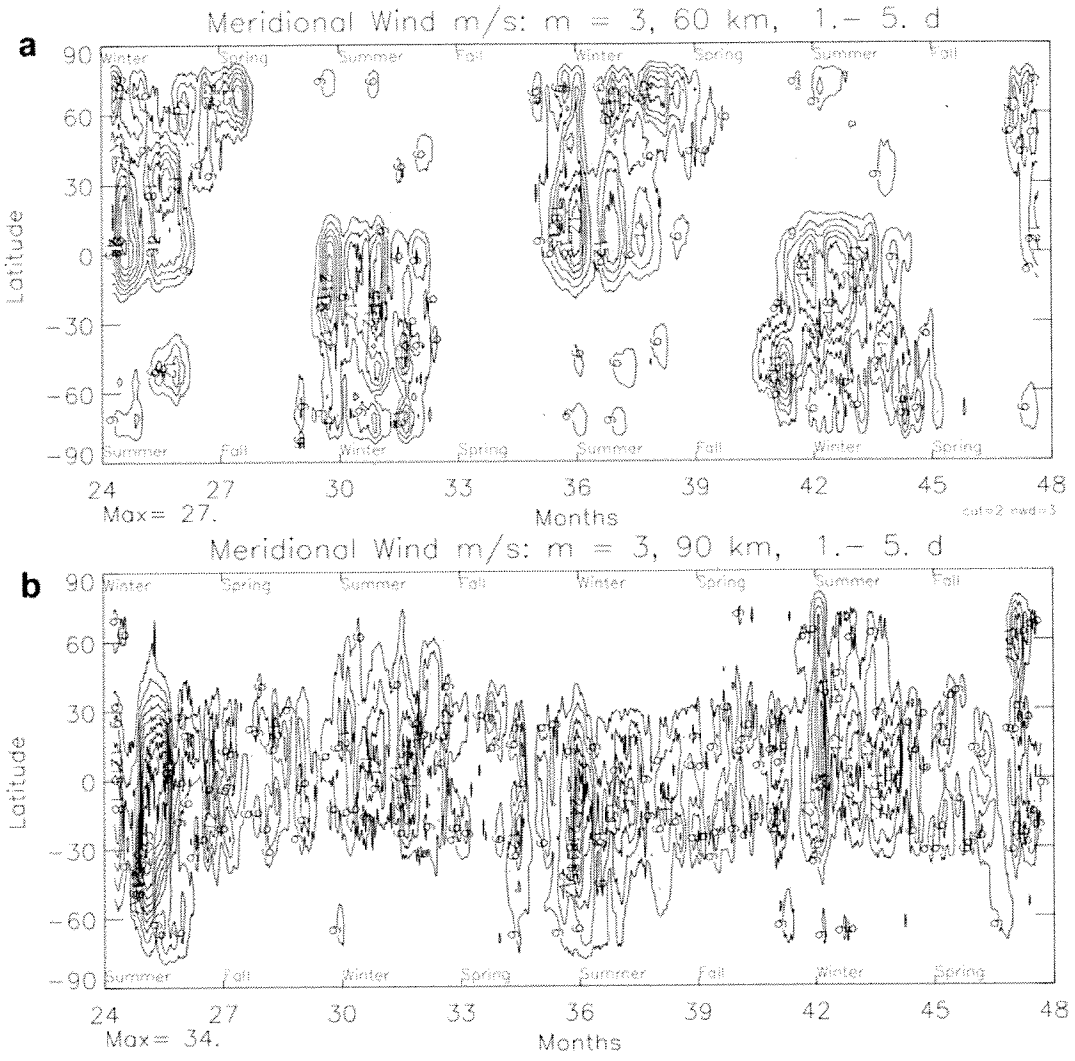
a
Meridional Wind m/s: m = 3, 60 km, 1.– 5. d
Winter
Spring
Summer
Fall
Winter
Spring
Summer
Fall
90
60
30
0
–30
–60
–90
Latitude
Summer
Fall
Winter
Spring
Summer
Fall
Winter
Spring
24
27
30
33
36
39
42
45
48
Max= 27.
Months
b
Meridional Wind m/s: m = 3, 90 km, 1.– 5. d
Max= 34.
Months

Figure 22

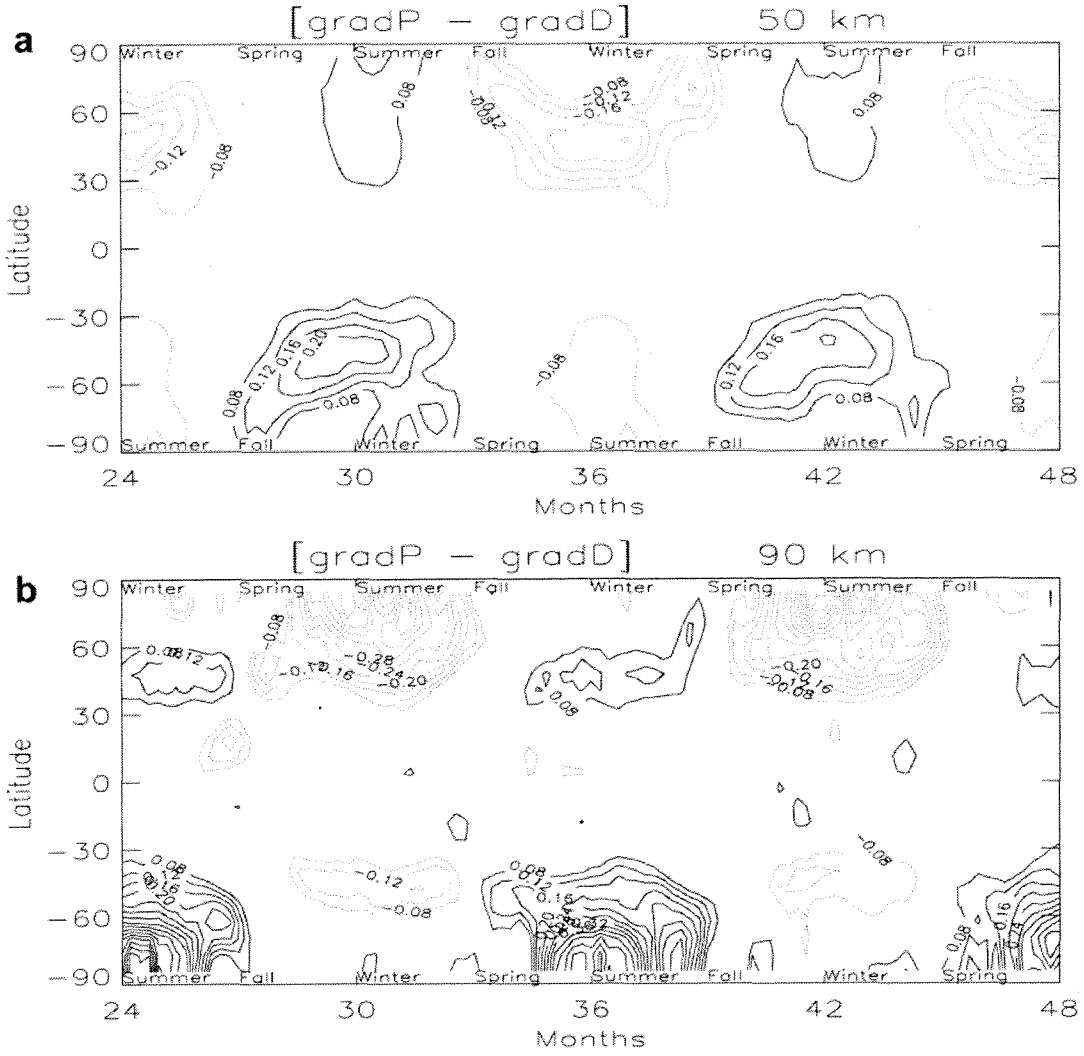
a
[gradP − gradD] 50 km
Winter Spring Summer Fall Winter Spring Summer Fall
90
60
30
0
−30
−60
−90
Latitude
Summer Fall Winter Spring Summer Fall Winter Spring
24 30 36 42 48
Months
b
[gradP − gradD] 90 km
Winter Spring Summer Fall Winter Spring Summer Fall
90
60
30
0
−30
−60
−90
Latitude
Summer Fall Winter Spring Summer Fall Winter Spring
24 30 36 42 48
Months

Figure 23